MEASUREMENT OF THE SPECTRAL DISTRIBUTION OF LOW ENERGY ELECTRONS EMITTED AS A RESULT OF NVV AUGER TRANSITIONS IN Ag (100)

by

SUSHANT KALASKAR

Presented to the Faculty of the Graduate School of

The University of Texas at Arlington in Partial Fulfillment

of the Requirements

for the Degree of

MASTER OF SCIENCE IN MATERIALS SCIENCE AND ENGINEERING

THE UNIVERSITY OF TEXAS AT ARLINGTON

December 2010

ACKNOWLEDGEMENTS

I would like to take this opportunity to thank the people who were instrumental in completion of my graduate studies and provide me with the much needed help in my research. The past two years at University of Texas at Arlington have been one of the most fulfilling and enriching ones in my life.

First, my heartfelt gratitude goes to my advisor and Department of Physics Chair, Dr. Alex Weiss, for his excellent guidance throughout my graduate thesis work at UTA. I was always inspired by his knowledge and even-mindedness. He gave me perhaps the best opportunity in my academic life by letting me perform the thesis experiments at the Brookhaven National Laboratory, New York. I am grateful for the research and teamwork experience that I gained at his UTA laboratory. I also thank him for providing me with multiple opportunities to present my work at different national and international schools and conferences.

I am also indebted to our collaborator, Dr. Steven Hulbert from the National Synchrotron Light Source at BNL. I was extremely motivated by his technical knowledge and skills combined with his ability to speedily tackle problems. He is very energetic and at the same time maintains a cheerful atmosphere at the lab. The fact that he trusted me with many of the NSLS beamline operations has always encouraged me in my research work at BNL. Thanks to Mr. Dong at the U1A beamline at BNL, who helped me in the beamline operations and got me acquainted with the work etiquettes and safety procedures at the national lab. I will always remember the exceptional research facilities provided to me at BNL, without which this thesis would be practically impossible to complete.

I am also grateful towards Dr. Robert Bartynski of Rutgers University, NJ for guiding us time-to-time through our work. Also my gratitude goes to the Welch Foundation for the necessary financial support towards this research.

I must also mention the professors at the Department of Materials Science and Engineering at UTA; Dr. Kim and Dr. Hao for providing me excellent theoretical knowledge which has always helped me understand the principles used in this thesis in a better way. I also express my sincere thanks to the office staff Margie Jackymack, Libia Cuauhtli and Jennifer Standlee, along with our technical experts Victor Reece and Doug Coyne. Also, I cannot forget my labmates Prasad, Karthik and Suman for always supporting and helping me selflessly throughout my research work.

My family and friends have always trusted me whole-heartedly ever since I remember. I express my gratefulness to my parents, Prakash and Sandhya, my brother Nishant and my sister-in-law Pallavi for everything that I have achieved till date. And life would be uninteresting without friends Neeraj and Harshada.

I again thank Dr. Weiss and Dr. Hulbert for this exceptional opportunity. I consider myself fortunate to have them as my guides.

November 22, 2010

ABSTRACT

MEASUREMENT OF THE SPECTRAL DISTRIBUTION OF LOW ENERGY ELECTRONS EMITTED AS A RESULT OF NVV AUGER TRANSITIONS IN Ag (100)

SUSHANT KALASKAR, M.S.

The University of Texas at Arlington, 2010

Supervising Professor: ALEXANDER HERMAN WEISS

Auger Photoelectron Coincidence Spectroscopy (APECS) was used to investigate the physics of the Low Energy Tail (LET) of the Auger spectrum of Ag (100) at the National Synchrotron Light Source, Brookhaven National Lab, New York. The incident photon energy was set at 180eV. The spectrum shows a peak due to the NVV Auger transition accompanied by a substantial low energy region. The APECS spectrum contains the contributions from electrons excited by the NVV Auger transition plus a background due to true coincidences between photo-emitted valence band electrons that undergo inelastic scattering and transfer part of their energy with other valence electrons which exit the sample. A series of coincidence measurements were made with the fixed analyzer set at energies 150,160,171.5 and 175eV. These measurements were used to obtain an estimate of the background due to the inelastically scattered valence band photoelectrons. The estimated background was then subtracted from the NVV APECS data to obtain the spectrum of electrons emitted solely as a result of the NVV Auger transitions, which contains implications for quantitative interpretation of the Auger spectrum.

TABLE OF CONTENTS

LIST OF ILLUSTRATIONS

Figure Page

LIST OF TABLES

CHAPTER 1

AUGER PHOTOELECTRON COINCIDENCE SPECTROSCOPY

1.1 Introduction

The experiments in this thesis were performed using the Auger Photoelectron Coincidence Spectroscopy (APECS) at the beamline U1A of the National Synchrotron Light Source (NSLS) at Brookhaven National Lab (BNL), New York.

Following principle is used in this technique. On making sufficient photon energy incident on an atom, the core level electron can be excited to be emitted out as a Photoelectron, thus generating a hole in the inner core shell. On getting highly excited due to the presence of a hole in the core shell, atoms relax often by Auger electron transition. In this process, a less tightly bound electron from a shell above the shell with the hole fills the shell hole. This excess energy is transferred to yet another neighboring electron which gets excited to get emitted from the atom. These electrons and their kinetic energies can be observed through the APECS spectrum peaks. These electrons on their way out get inelestically scattered and get emitted with lower kinetic energies. A low energy tail is formed as a result of these electrons which dominates the photoemission spectra of solids. In the experiments conducted we have tried to simplify the Low Energy Tail (LET). We remove the unrelated background LET emission leaving behind only pure LET given by the emission of the core photo-electrons.

The Low energy tail (LET) dominates the photoemission spectra of solids. This tail is composed of inelastically scattered valence, core, and Auger electrons as well as electrons emitted after multiple inelastic scattering events. The LET extends from the lowest measurable electron kinetic energies (~2eV) up to ~15eV. Since the LET is causally related to all primary photoemission features, time coincidence measurements between any of these primary features and the low kinetic energy region results in a strong LET that dominates the coincidence

(APECS) spectrum. The APECS LET spectrum does not contain any LET emission originating from primary features other than the one selected by the fixed electron energy analyzer. For example, if the fixed enery analyzer is set to the Ag 4p core photoelectron peak, the APECS LET contains only decay features of that core excitation process, i.e. Auger emission peaks and inelastically scattered 4p electrons. In this way, the Ag 4p NVV APECS spectrum reveals the Ag NVV Auger peak which is swamped by secondary electron emission in the non-coincidence LET spectrum. In practice, the Ag 4p photoelectron peak sits on top of LET emission from higher kinetic energy photoemission or Auger emission peaks. Therefore, the measured Ag 4p NVV LET contains a significant fraction of LET emission coincident with the background emission at the Ag 4p photoelectron kinetic energy, but unrelated to the Ag 4p excitation event. We would like to separate the Ag 4pNVV APECS LET from this background LET, leaving only the "pure" Ag LET spectrum created by excitation of Ag 4p photoelectrons only. This separation cannot be accomplished via APECS, since the fixed channel contains indistinguishable contributions from Ag 4p photoelectrons and inelastically scattered background emission. One method for estimating the background LET spectrum is to extrapolate it from measured APECS LET spectra for fixed analyzer energies at selected kinetic energies higher than the Ag 4p photoelectron peak. The algorithm is to determine the trend vs. fixed kinetic energy of these non-APECS LET spectra. At 180eV photon energy, the Ag 4p photoelectron peak is seen at 133 eV. We measured the Ag 4p NVV APECS LET spectrum at this fixed energy and at a few kinetic energy values higher than 133eV, up to the valence band seen at 186.7 eV electron kinetic energy. We chose to measure background APECS LET spectra at the following fixed analyzer kinetic energy values: 150, 160, 171.5, 175 and 186.5 eV, where the final value is in the middle of the Ag valence band.

1.2 Electron Emission Processes

1.2.1 CVV Auger Transition

An atom is excited by having a hole in the core level by using photons of energy h*v* incident on the sample. This Synchrotron radiation energy used, hv, is slightly higher than the binding energy of the core electron, E_C. This core hole is filled by an electron from the valence

band, with binding energy is E_{V1}, thus neutralizing the excited atom. This transition energy, which is the difference in the binding energies of the core and the valence electron, is preferably released by Auger electron (with binding energy E_{V2}) emission. The transition energy can be released as X-Ray emission if the binding energy of the core electrons is >2 keV and in this case there won't be an Auger emission.

Direct Auger decay or CVV Auger decay is as shown in the Figure 1.1. [1-2] Thus in the end, the atom will be left with two holes in the valance band. The kinetic energy of the emitted Auger electron is given by the Equation (1) below:

$$KE_{CVV} = E_C - E_{V1} - E_{V2} - \phi_A \quad (1)$$

Here, ϕ_A is the work function of the Cylindrical Mirror Analyzer. E_C is the binding energy of the core at its original position and all energies in the equation are in reference to the Fermi level of the solid. The binding energies of the two electrons involved in the Auger transition are given by E_{V1} and E_{V2}. For the Fermi level electrons,

$E_{V1} = E_{V2} = 0$ eV.

Thus, for CVV Auger electrons, as per Equation (1), the Auger electrons emitted from the Fermi level will carry the maximum energy $KE_{CVV(max)} = E_C - \phi_A$.

For the minimum CVV Auger energy, both the electrons should be coming from the bottom of the valence band. The Kinetic Energy of these electrons will be given by $KE_{CVV(min)} = E_C - 2W - \phi_A$

The energy width can be estimated using the above equations, and is given by Equation (2) below,

$$\Delta KE_{CVV} = KE_{CVV(max)} - KE_{CVV(min)} = 2W \quad (2)$$

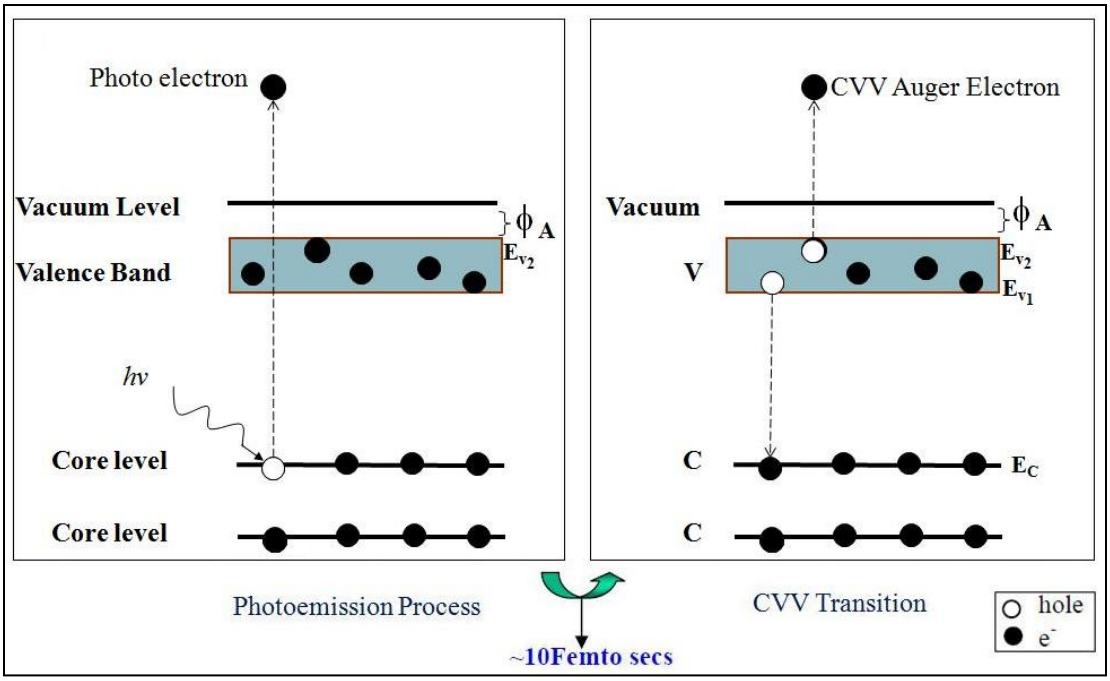

Figure 1.1 Energy level diagram showing direct CVV Auger emission

1.2.2 Inelastic Scattering of Valence Photo-electrons

The low energy tail (LET) region of the photoelectron spectrum shows dominant contributions from inelastically scattered valence, core and Auger electrons as well as electrons emitted after multiple inelastic scattering events.

In an inelastic scattering event of a Valance electron, an atom is excited by having a hole in the valance level by using photons of energy hν incident on the sample. The outgoing valence band photo-electron leaves the atom with a kinetic energy given by the equation:

$$KE_{Valence} = h\nu - E_{V1} - \phi_A \quad (3)$$

Suppose that in an event of inelastic scattering of this outgoing photo-emitted valance band electron, it transfers an energy **Δ** is transferred to another neighboring valance band electron. Thus, now it gets emitted with an energy reduced by a value of **Δ**. Thus, from equation (3) we have,

$$KE_{InelasticValence1} = h\nu - E_{V1} - \Delta - \phi_A \quad (4)$$

Inelastic scattering event of photo-emitted valance band electrons is as seen in the Figure 1.2.

For the Conservation of Energy principle to be satisfied, in this inelastic scattering event the other valance electron which accepts energy ≤ **Δ** eV from the photo-emitted valence electron and leaves the atom with a kinetic energy given by the equation:

$$KE_{InelasticValence2} \leq \Delta - E_{V1} - \phi_A \quad (5)$$

Where the less than or equal sign reflects the fact that the electron can lose some of its own energy through additional inelastic processes. These inelastically scattered valence band photo-electrons form a major portion of the Low Energy Tail (LET) region of the Photoemission spectra of solids.

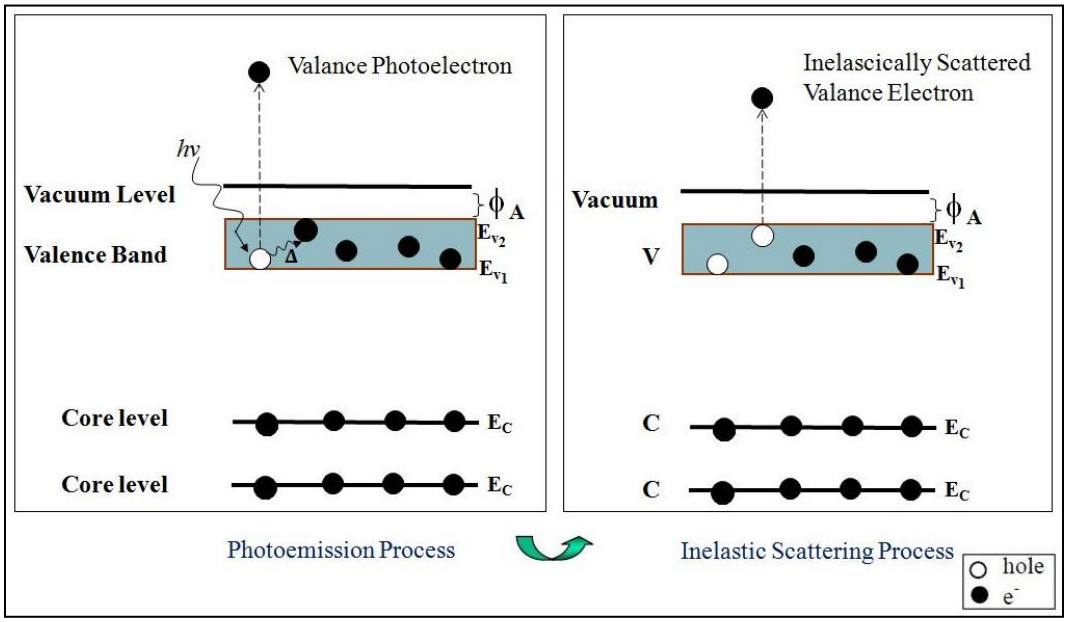

Figure 1.2 The Inelastic Scattering of Valence band photo-electrons

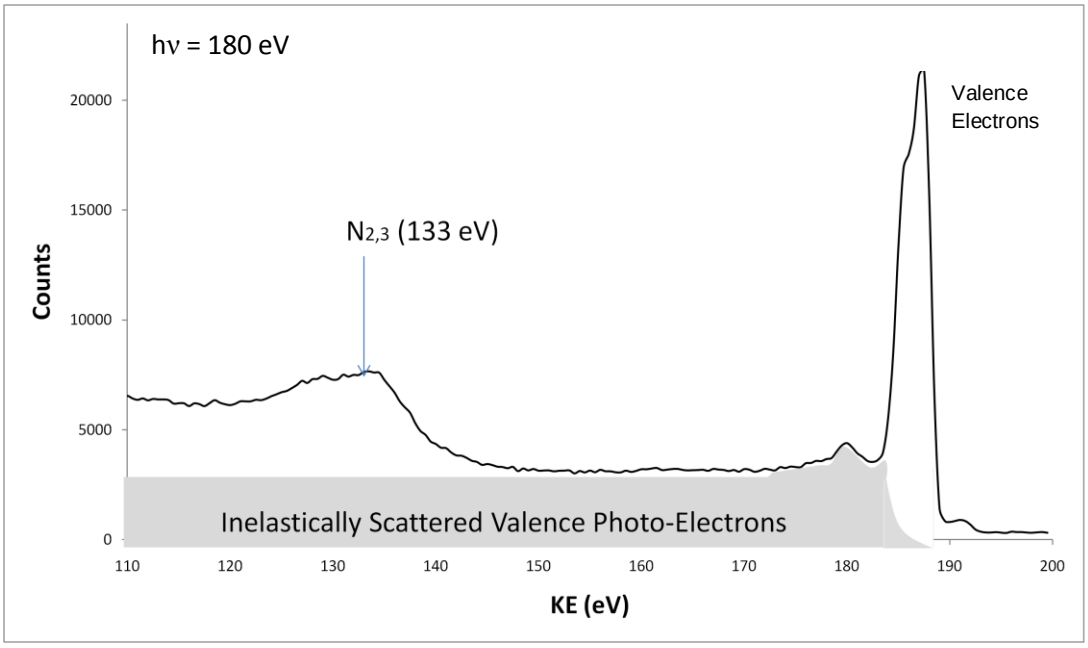

Figure 1.3 The Photoelectron spectrum for Ag at hν = 180 eV (with -15V Sample Bias). The assumed contribution of the inelastically scattered valence band photo-electrons to the spectrum is shown schematically by shaded region

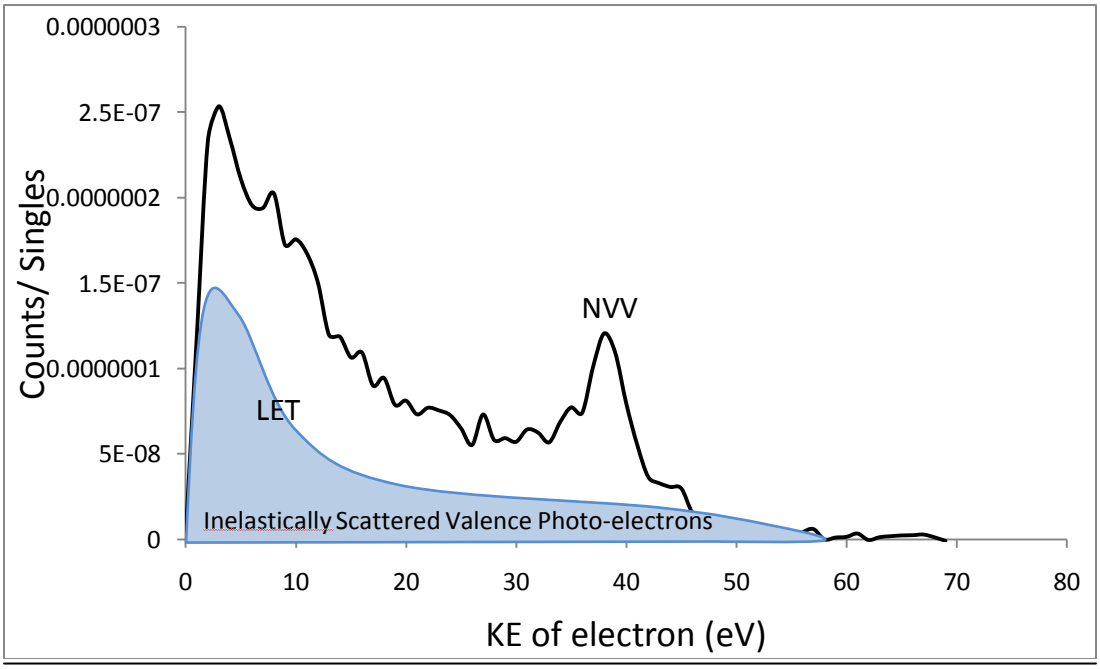

Figure 1.4 Normally observed Ag CVV Auger spectrum. The observed Low Energy Tail (LET) is indicated. Estimated contribution to the LET by the inelastically scattered valence band photoelectrons is shown schematically by shaded region

1.3 Quantification of the APECS spectrum

Ever since the earliest applications of Auger Electron Spectroscopy, efforts were devoted to improving quantification. The quantification technique mentioned below is used in many AES and XPS commercial instruments used for industrial applications.

The starting point is the linear equation given by M. P. Seah et al. [17], showing that the intensity of the signal, I_A, from element A in a solid is proportional to the molar fractional content, X_A, in the depth to which the sample is being analyzed. The expression is given by the equation (6) shown below,

$$X_A = \frac{I_A}{I_A^\infty} \tag{6}$$

Here, I_A^∞ is the sensitivity factor, it being the intensity from pure A. Usually the value of I_A^∞ is not known, but the value of I_A^∞ / I_B^∞ if known, can be used in the equation (7) shown below, where B is some other constituent of the solid:

$$X_A = \frac{I_A / I_A^\infty}{\sum_{i=A,B} I_i / I_i^\infty} \tag{7}$$

Here, the sum is overall of the solid constituents.

The terms contributing to the I_A value can be determined for the APECS technique. In the APECS spectrum the measured Ag 4p NVV LET contains a significant fraction of LET emission coincident with the background emission at the Ag 4p photoelectron kinetic energy, but unrelated to the Ag 4p excitation event. This includes emission due to inelastic scattering of the Auger and valence electrons along with multiple electron Auger emitted by sharing the Auger energy. We would like to separate the Ag 4pNVV APECS LET from this background LET, leaving only the "pure" Ag LET spectrum created by excitation of Ag 4p photoelectrons only. This would help in determining the I_A value which is characteristic only to the Auger transitions and thus result in a better quantification of the acquired data.

1.4 Sample Description

The sample used in the APECS calculations is Ag (Silver).

It is a single crystal with crystal orientation of (100).

Ag Atomic Number: 47

Electronic Structure: 1s2, 2s2, 2p6, 3s2, 3p6, 3d10, 4s2, 4p6, 5s1, 4d10

Table 1.1 Binding Energies of Core level electrons for Ag [3]

Shell	Sub shell	Binding Energies (eV)
K	1s	25514
L_I	2s	3806
L_{II}	$2p_{1/2}$	3524
L_{III}	$2p_{3/2}$	3351
M_I	3s	719
M_{II}	$3p_{1/2}$	603.8
M_{III}	$3p_{3/2}$	573
M_{IV}	$3d_{3/2}$	374
M_V	$3d_{5/2}$	368.3
N_I	4s	97
N_{II}	$4p_{1/2}$	63
N_{III}	$4p_{3/2}$	58

CHAPTER 2

APECS INSTRUMENTATION

2.1 Introduction to Synchrotron Radiation

Synchrotron Radiation is an electromagnetic radiation emitted by charged particles moving in relativistic velocities along a curved trajectory. The trajectory has a large radius of curvature. Synchrotron radiation has many important characteristics which make it a unique spectroscopy tool, including: High intensity, Broad spectral range, Pulsed time structure, High polarization and so on. The electron accelerator emits synchrotron radiation in form of photon energies over a broad range. These energies are from gamma rays and hard x-rays to microwaves photon energies. Also, the synchrotron radiation produced in an electron storage ring occurs with ultra-high vacuum, a small spot size and stability. All these properties make synchrotron radiation a unique spectroscopic tool. [4]

The Synchrotron Radiation due to all these properties is an important experiment tool. The Photon energy used falls in the range 10^{8} to 10^{-1} A^{o}. The lengths of chemical bonds, lattice constants, atomic and molecular sizes fall in this range. Thus, the photons from the Synchrotron radiation can be used in the study of atomic and molecular structures in solids, due to their appropriate wavelength.

The binding energies of electrons in atoms and molecules correspond to the energy of photons, which ranges from a few meV (IR) to 10^{5} eV (x-ray). The electrons bound in the atoms and molecules include valence electrons, core electrons and the electrons which are involved in chemical bonding. Synchrotron radiation photon energy can be thus used to analyze the properties of these electrons and the chemical bonds they are involved in. Physical and chemical properties can be probed by using the knowledge of these electrons and their bonding.

2.2 Storage Ring

The experiments presented in this thesis have been performed on the U1A beamline at the National Synchrotron Light Source (NSLS), Brookhaven National Laboratory (BNL), New York. The NSLS is a Department of Energy (DOE) funded research facility dedicated to producing intense UV and X-Ray light.

Photoelectron and Auger electron spectroscopy provide us information on the energies, electronic structure of atoms and molecules. [5,6]

2.2.1 Storage Ring Components

1. Vacuum Chamber: The electrons circulate in this metal tube in a closed trajectory. It is a metal tube with typical pressure of 10^{-10} to 10^{-11} Torr.

2. Dipole Bending Magnets: The trajectory of electrons is bent by these magnets. It thus aids the electrons to circulate in closed orbit inside the vacuum chamber.

3. Injection: The electrons are generated, accelerated and then injected by this injection system into the storage ring.

4. RF Cavities: The circulating electrons lose energy due to the emission of synchrotron radiation. The RF cavity system restores the energy lost by these electrons periodically.

5. Focusing magnets: Dipole and quadrupole magnets act as the focusing magnets for the electron beam injected in the storage ring.

6. Insertion devices: The trajectory of the electrons is modified in the straight sections of the ring by a periodic array of magnets. This leads to the emission of synchrotron radiation.

7. Computer controls: Required changes in the status of the ring components can be made automatically or semi-automatically through the computer system. The system monitors the various beam components and their functioning.

8. Shielding system: The shielding system blocks harmful radiation from reaching the user facility area. The harmful radiations emitted out include neutrons and gamma rays.

2.2.2 NSLS Ring

Two electron storage rings are operated at the NSLS, viz. the VUV ring and the X-Ray ring. [See Figure 2.1] The electrons are injected into the NSLS storage rings from a 750MeV booster synchrotron fed by a 120MeV LINAC. Intense focused light ranging from infrared to X-Ray electromagnetic spectrum can be obtained using these rings. The linear accelerator (LINAC) injects the electron beam into the synchrotron, which then injects the beam into the NSLS storage ring. This NSLS injector LINAC contains various parts to generate, accelerate and shape the electron beam to be injected into the booster synchrotron. These parts include the electron gun, the low energy beam transport system (LEBT) accelerating cavities, the radio frequency (RF) system and its beam transport system. The electrons from the electron gun are bunched together by applying appropriate voltage. [6] Using the low energy beam transport system, the electrons can be transferred to the booster ring.

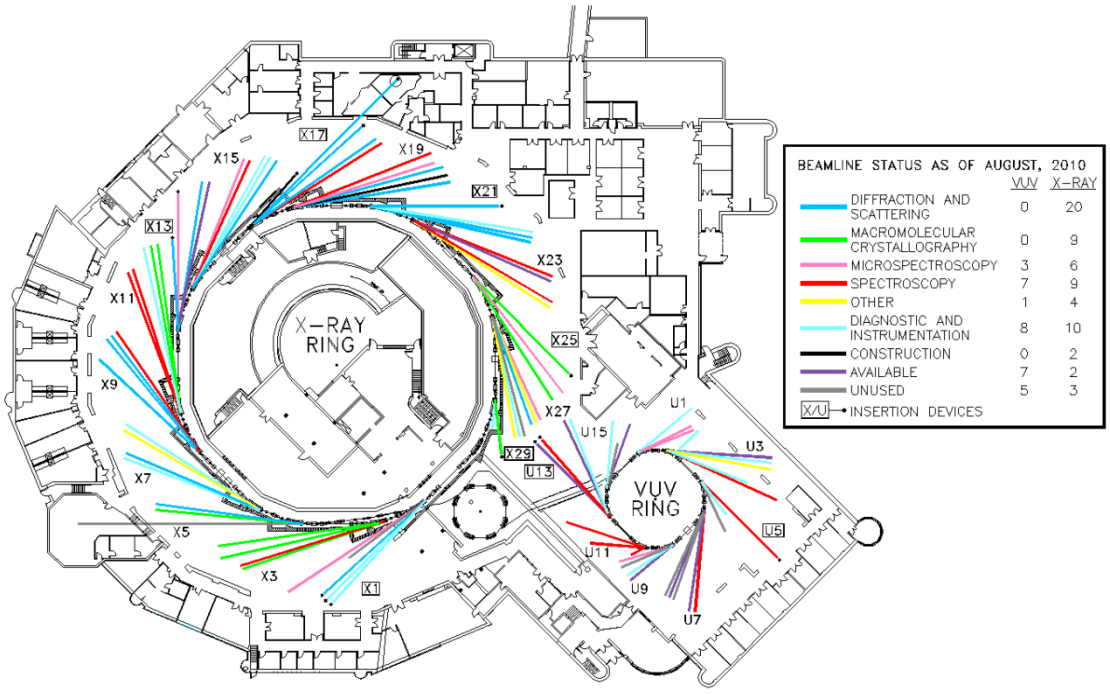

Figure 2.1 The VUV ring and the X-ray ring, Floor plan of the National Synchrotron Light Source

Now, the RF fields provide these electrons with voltage that accelerates the electrons to about 116 eV. Quadrupoles help in focusing and guiding these electrons, thus preventing radiation emitted due to rejected electrons. Thus, the electrons are focused in both horizontal and vertical directions and the beam is shaped. The bending of the beam around the corners is achieved by the dipole magnets. The beam is injected into the booster ring and the RF accelerating cavities increase the energy of the electrons to 750 MeV. Upon reaching this energy, the electrons are fed to either the VUV or the X-Ray ring at the NSLS. In the VUV ring, out of the total of 9 bunches orbiting simultaneously at 800 eV energy, 7 are filled. The storage ring gets filled up to a desired operating current by this electron injection. The electrons are made to orbit around the ring by 8 dipole bending magnets. Synchrotron light is released when the circulating electrons lose energy at each bend. The RF (52.89 MHz) cavities supply energy to the electrons in the ring again. At each bend, two beam ports are positioned. When the shutters at these two beam ports are opened, synchrotron light in the VUV region is emitted out and passes through the beamlines to reach the sample endstation.

2.3 Beamline U1A

The Synchrotron radiation emitted by the Storage ring is transferred till the end station through the beamline. [See Figure 2.2] It consists of several critical components which are discussed below:

1. EGR Monochromator : Photons of only the desired energy are allowed to pass through by the monochromator. It eliminates the photons of all other energies. The EGR Monochromator is discussed in more details further in this chapter.
2. Mirrors: High optical quality of the photon beam is preserved by the mirrors by focusing and refocusing the photons as they travel through the beamline.
3. Vacuum generation system: A combination of number of vacuum pumps is used to get the desire 10^{-10} Torr pressure. Ultra high vacuum along the beamline is necessary to avoid absorption losses as the radiation is transmitted through the beamline. Also, it is important to keep the beamline pressure compatible with that at the endstation and the storage ring.

4. Ultra High Vacuum Endstation: The experiment chamber is designed specific to the experiment requirement.
5. Controls System and Computers: Controls system controls the monochromator and the vacuum system.
6. Other components which are necessary for the effective operation and working of the beamline are beam supporters, baffles, collimators, filters. etc.

2.3.1 Beamline Components

All data reported in this thesis has been taken at the National Synchrotron Light Source (NSLS) Vacuum Ultraviolet (VUV) ring on beamline U1A.

The U1A beamline components consist of a horizontally-deflecting focusing mirror followed by a vertically-deflecting mirror and a vertically-dispersing VUV/soft x-ray monochromator of the Extended Range Grasshopper (ERG) type [7]. The focused beam at the exit slit of the ERG propagates downstream to a 1:1 refocusing mirror that focuses on the sample in the experimental endstation. The VUV ring and the U1A beamline are pumped to ultra-high vacuum (UHV) in order to minimize contamination, by carbon, of the optical elements.

2.3.2 The Ultra High Vacuum Endstation

The experimental endstation [See Figure 2.2] consists of a vacuum chamber, pumps to maintain ultra-high vacuum, an x, y, z, θ sample manipulator, two electron energy analyzers, and associated instrumentation such as electron gun, sputter ion source, leak valve and gas lines.[8] The electronics for this endstation include a current meter to measure the sample-to-ground current, a sample bias voltage source, the electron energy analyzer controllers, channeltron detector electronics, and coincidence electronics, described below. The focused synchrotron radiation (SR) beam from the U1A beamline is incident normally on the sample surface in the experimental endstation after entering this UHV chamber horizontally midway between the two electron energy analyzers. During data acquisition, the focused SR beam, the sample surface, and the source points of both electron energy analyzers must be aligned to overlap as completely as possible.

The UHV chamber is a typical ion and turbo-molecular pumped chamber made out of stainless steel. Ultra-high vacuum as high as mid-10^{-11} Torr routinely can be achieved in the chamber with overnight bakeouts. The chamber has two 8 in. ports which are oriented at 145° from each other on a plane 10° below horizontal, in which the two electron analyzers are mounted. The chamber is placed on an adjustable mounting table in order to align the electron energy analyzer source point with the SR beam. The sample is mounted on a manipulator which has 4 degrees of freedom to move (x, y, z, and θ) in order to place the sample surface in a plane normal to the incident SR beam that is aligned with the electron energy analyzers. . One of the electron energy analyzers is fixed to the endstation chamber and is aligned by adjustment of the chamber mounting table, while the second analyzer is connected to this chamber by a UHV bellows and three adjustment screws that provide linear adjustment along the analyzer axis and angular adjustment in a place perpendicular to this axis. The simultaneous alignment of beam, sample, and both analyzers is critical, as the maximum achievable count rate is determined by the degree to which the two analyzers image the same sample surface volume. The energy resolution of the analyzers depends on the size of their apertures, which can be adjusted either to the large or the small setting by the turn of a knob. For the small (large) aperture setting the analyzer energy resolution is 0.6% (1.6%) of the analyzer pass energy, which in turn is related to the voltages applied to the inner and outer cylinders of these Double-pass Cylindrical Mirror Analyzers, which are on the order of a few 10's of volts. In the coincidence measurements, we utilized large apertures, while for taking high statistics photoemission spectrum we used small apertures with lower pass energy in order to achieve better electron energy resolution.

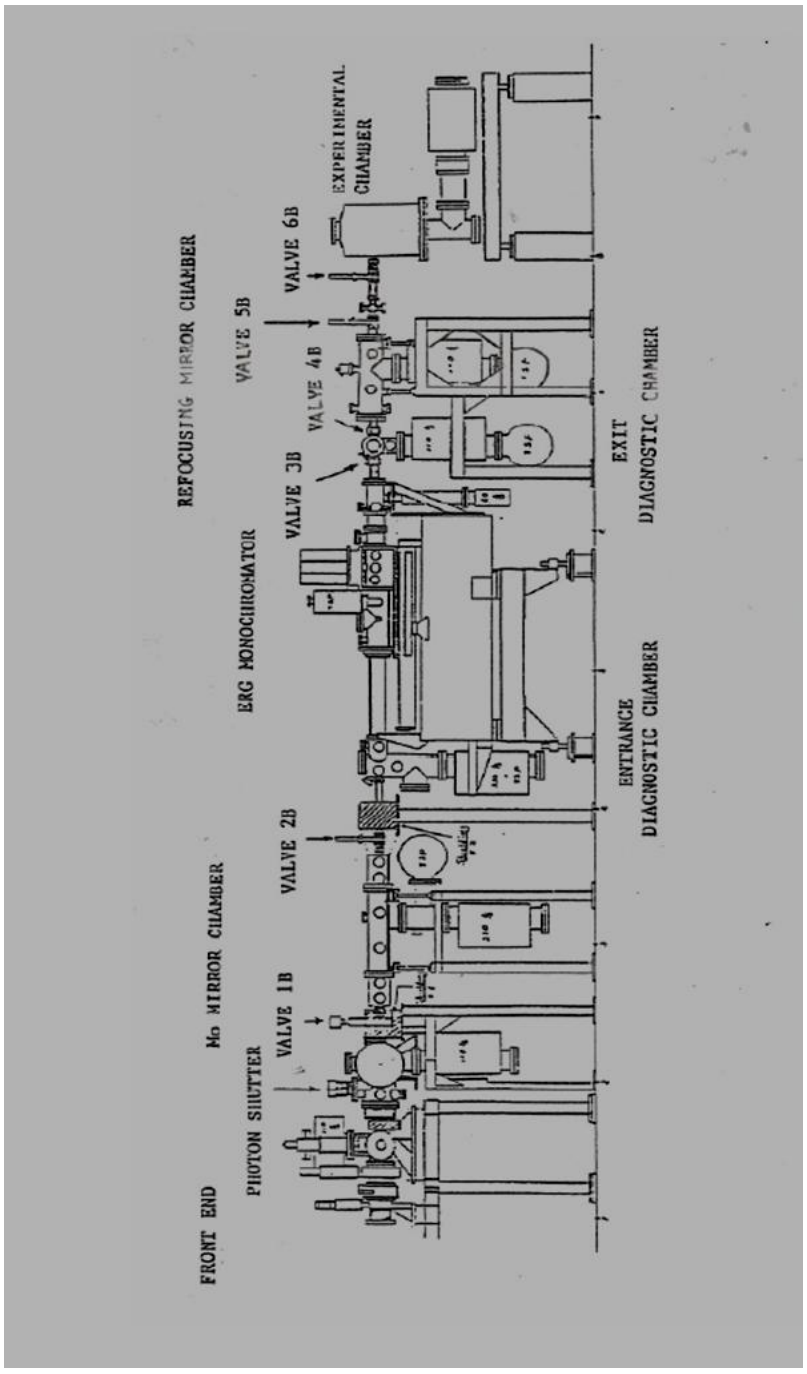

Figure 2.2 Diagram for Beamline components for U1A, NSLS, BNL

2.3.3 Vacuum Generation components

Pfeiffer TPU-050(50- L/S) Turbo Molecular Pump is backed up by Varian SD-90, a rotary vane mechanical pump. Once the pressure reaches 10^{-6} then, the Ion pump Perkin Elmer Model # 2070122 (120 L/S) brings the pressure into the 10^{-10} Torr range.

2.4 Cylindrical Mirror Analyzer (CMA)

Two Cylindrical Mirror Analyzers are used in the experiment. These are double pass cylindrical mirror electron-energy analyzers (PHI Model 15-225G) [11], each installed in an eight inch port. They are oriented 145º from each other and at a plane 10º below the horizontal plane. Each CMA consists of the following important components: a) Internal electron gun, b) Channeltron, c) Analyzer, d) Variable aperture, e) Radiation grid. The Figure 2.3 shows the aperture controls and the flange-mounted terminals on the CMA used.

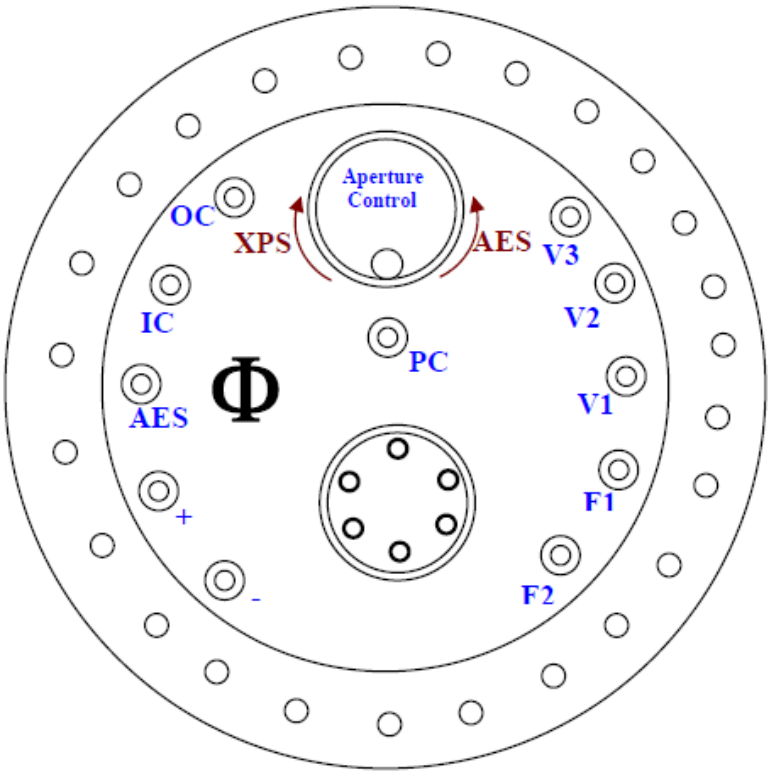

Figure 2.3 CMA aperture controls [16]

The electrons travel in the space between the inner and outer cylinders. Apertures, located on the cylinder axis, are located at the foci of the first and second analyzer stages (passes). The apertures are switched to either small or large size by rotating the knob at the back of the CMA flange. The distance between this flange and the specimen under study is critical for the accurate measurement of the kinetic energy of the electrons entering the CMA. This distance is 27.94 cm in the experiment setup used. The electron gun present in the CMA is not used as the photons from the Synchrotron ring are used to trigger the Auger electron emission from the sample.

2.4.1 CMA Controller Power Supplies

The power supply units which help to control the IC and OC voltages in the CMAs is as seen in the Figure 2.4:

a) Offset Supply

It is a power supply with an output 0 – 500 V DC that is linearly proportional to the (0 – 10 V DC) input from CAMAC D/A module. It consist of two programmable power supplies which are used to set the retarding voltage of the CMA's that select the energy of the electrons which pass through the CMA. The meters in the front indicate the voltages set for the RCMA and LCMA. It is termed as V_{Ramp}. This voltage is always set to negative.

b) Extra Power Supplies

The offset power supply described above has a scan range of 0 – 500 V. If a core electron from the sample is being emitted out with a binding energy higher than this value, the energy of interest can be above 500 V. To achieve this, an additional DC voltage supply can be added.

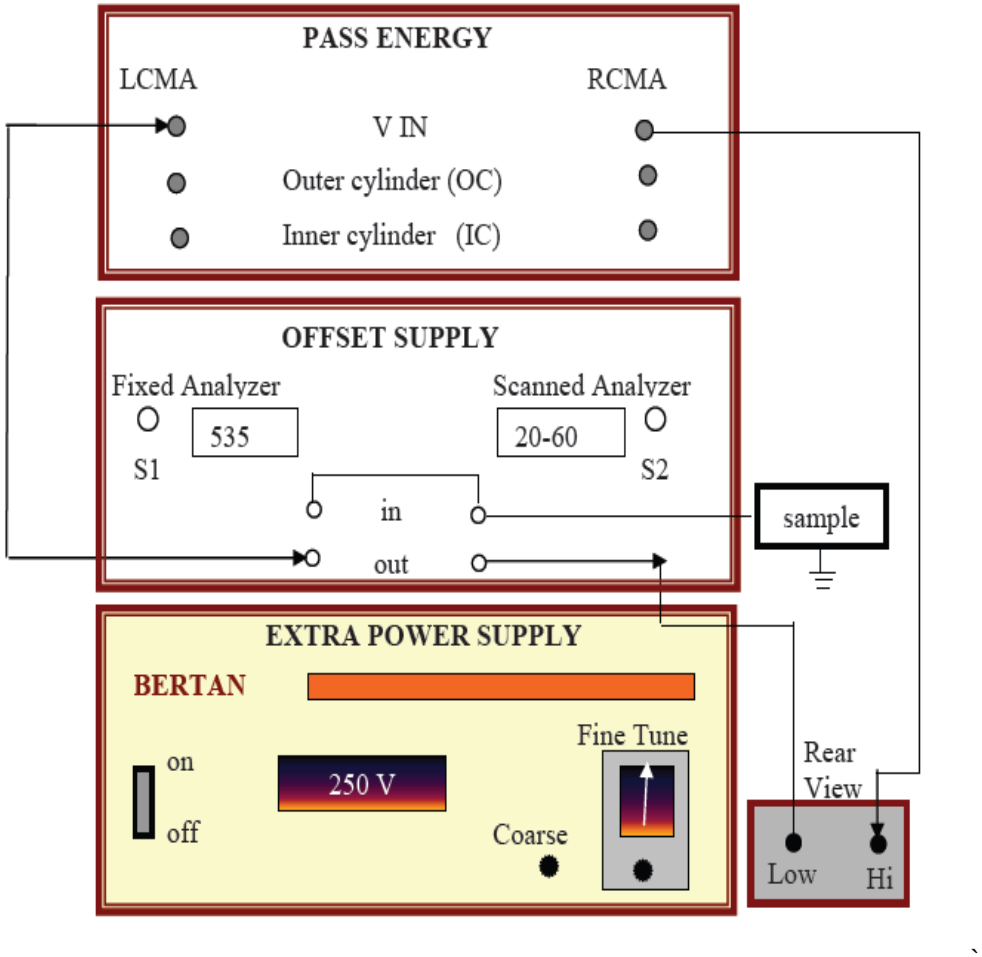

Figure 2.4 Block diagram of power supply unit to set the voltages on the IC and OC of the CMA [16]

2.5 Electron Energy Analyzer and Detectors

The electrons knocked out from the sample surface in the experiment are released in all the possible directions. The CMAs are used to detect these electrons which are released at an angle 48° ± 5° to the analyzer axis.[7] The outer cylinder is negative biased compared to the inner cylinder, since the inner cylinder is set to attract the electrons. This leads to the formation of a radial electric field in the space between the two cylinders, with the negativity increasing gradually towards the Outer Cylinder. Thus the electrons entering the CMA will get attracted more towards the inner cylinder (IC) compared to the outer cylinder (OC) and get deflected towards the axis of

the CMA. The Negative voltage on OC will deflect the electrons towards the IC and these electrons can now pass through the slits on the IC to enter the electron multiplier. Although the electrons getting into the CMA with energy higher than the pass energy will strike on the walls of the OC, the electrons with energy lower than the pass energy will hit the IC and thus not enter the CMA. Thus, only the electrons which satisfy the pass energy will succeed in entering and passing through the gap between the two cylinders. The deflection of these electrons by OC depends on the kinetic energy of the electrons as well as the voltages applied at the OC and IC. A second stage of filtering is induced by using the 'double pass' type design. This filtration can help in avoiding the secondary electrons generated internally in the analyzer.

The energy of the electrons entering the openings of the IC is amplified by the Chaneltron electron multiplier, thus making it possible for the electrons to reach the collector plate. The amplification of the signal is to the range 10^6 - 10^7 to generate a signal which can be measured by the collector plate. Higher the voltage applied, higher will be the attraction of the electron towards IC. In this manner, the kinetic energy of the electron is controlled by fixing the pass energy of the analyzer. The expression for the pass energy is given by, $E_{Pass} = 1.7\ (V_{IC} - V_{OC})$.

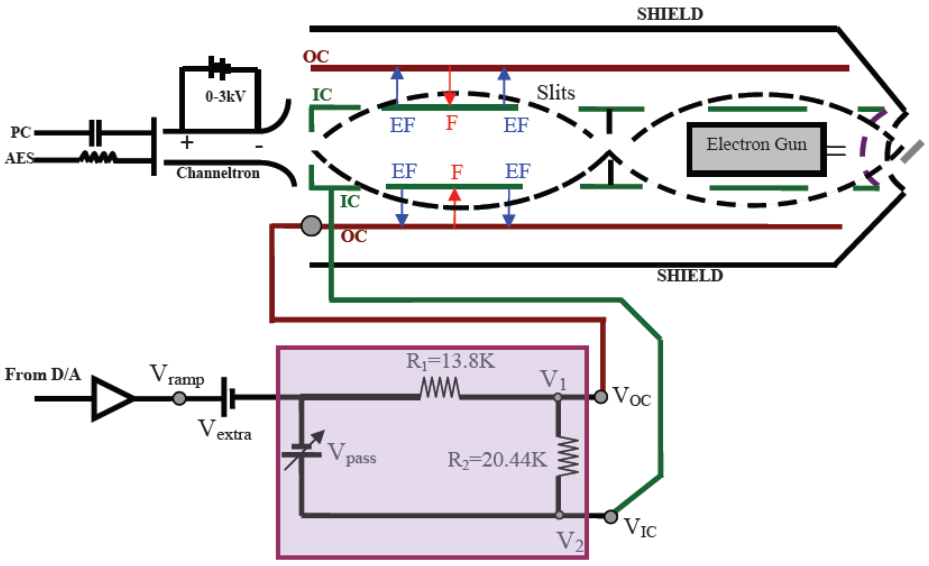

Figure 2.5 Schematic diagram of CMA and Power supply for Inner and Outer Cylinder

The aperture diameter affects the resolution and the luminosity. For higher resolution, the aperture is set to small. With a large aperture, the resolution is not high, but a lower signal to noise ratio can be achieved.

2.5.1 Pass energy of the CMA

The voltages of the IC and OC are set and only the electrons which match the pass energy of the CMA would pass through it making it to the channeltron and thus get detected. The outer cylinder is always set at a voltage more negative than the inner cylinder. The Figure 2.6 shows the circuit diagram of the circuit for pass energy.

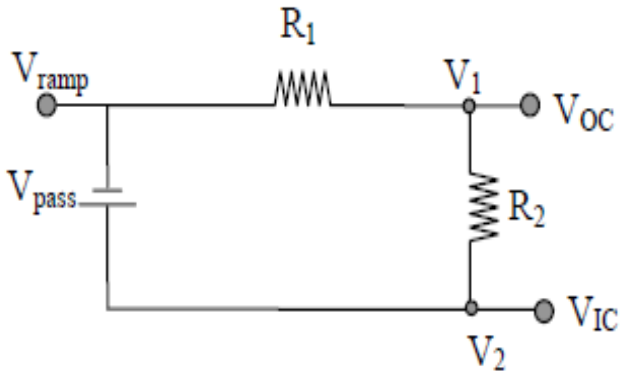

Figure 2.6 Circuit diagram for Pass Energy of CMA [16]

The Equations below, give the expression for the voltages on IC and OC to achieve the desired pass energy.

$V1 = V_{OC} = V_{Ramp} + \left(\frac{R_1}{R_1 + R_2}\right) V_{Pass}$

$V2 = V_{IC} = V_{Ramp} + V_{Pass}$

2.5.2 Electron detection and Coincidence electronics

The Figure 2.7 shows the CMA electronics involved in the coincidence experiment. The CMA is basically used to detect and count the number of electrons entering the CMA with specific kinetic energies. This CMA output is then sent to an amplifier and discriminator device. Next in the circuit is the TAC (Time to Amplitude converter) which receives the amplified and

discriminated output as a start signal. This TAC device now, gives a signal out which has an amplitude which is proportional to the difference between the start and stop signal. This signal will have a height which is recorded as a histogram in the MCA.

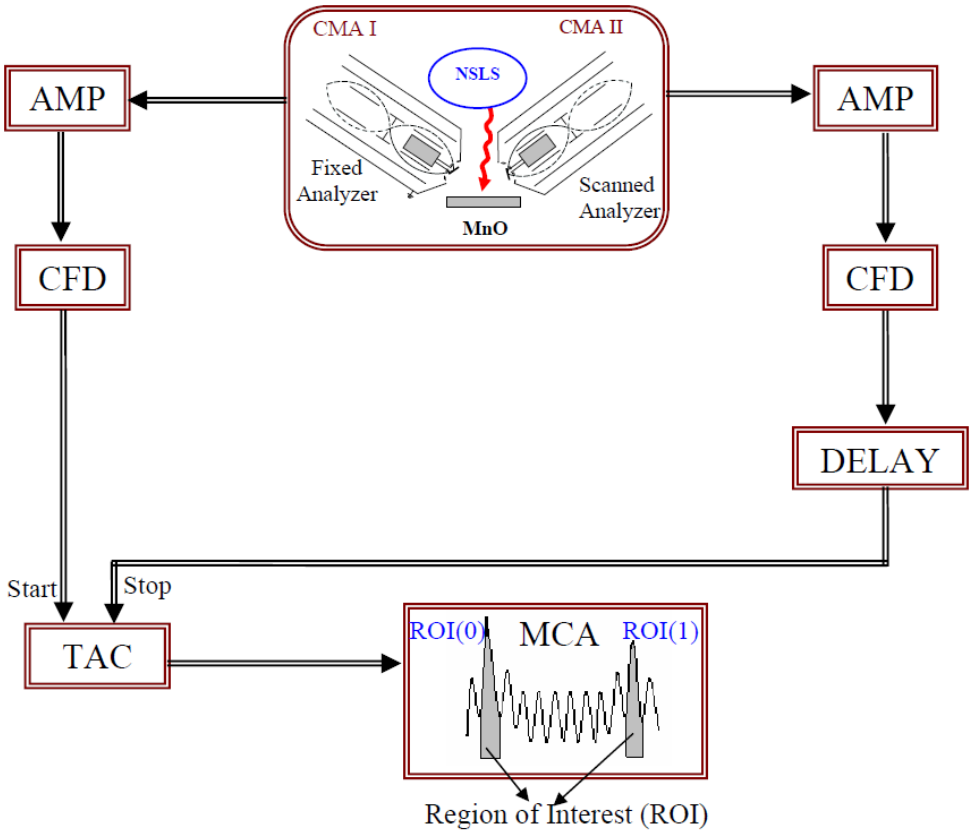

Figure 2.7 Schematic showing the electronics used in the coincidence experiment [16]

The output of each CMA is directed to an amplifier and a discriminator. The amplified and discriminated signal from one CMA is used as the start signal of a time-to-amplitude converter (TAC). The signal from the second CMA is also amplified, discriminated and fed through the delay circuit to bring the data into the positive time regime, and this is used as a stop signal to the TAC. The TAC outputs a signal whose amplitude is proportional to the time interval **Δ**t between the start pulse (electron arrival in CMA 1) and the stop pulse (electron arrival in CMA 2). The time

amplitude pulses are recorded as a histogram in the MCA wherein pulses having a particular height binned in the corresponding timing channel. [See Figure 2.8]

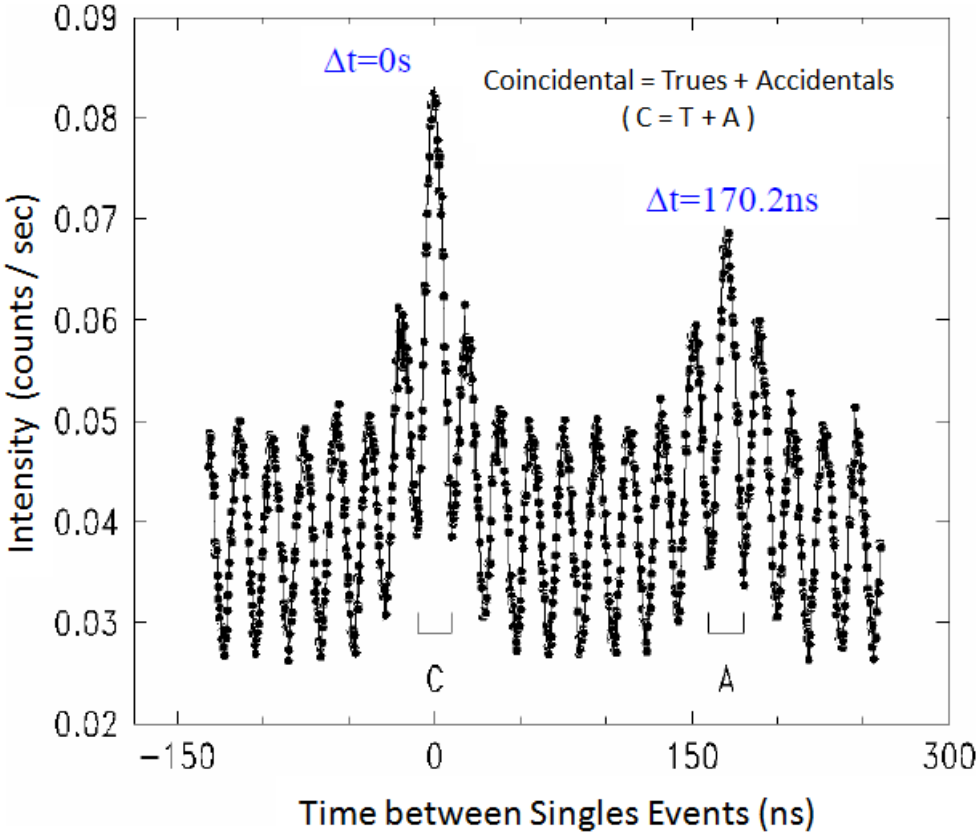

Figure 2.8 MCA Timing Spectrum [16]

The timing structure of the Synchrotron bunches in the VUV ring is evident from the timing spectrum recorded by the MCA, which consists of a train of 9 buckets, each ~10ns wide, evenly spaced by 170.2ns/9 = 18.9ns, where 170.2ns is the revolution period around the ring. If the 9 buckets were evenly filled, all the MCA peaks would have equal amplitude, except the Δt = 0 ns peak. However, only 7 of the 9 buckets are filled, and the 2 empty buckets are adjacent to each other, resulting in variation in amplitude of the MCA spectrum with a 170.2ns period. With an assumption of equal electron occupation for all the 7 filled electron bunches, the envelope

function follows the repeat pattern: 7/9, 6/9, 5/9, 5/9, 5/9, 5/9, 5/9, 5/9, 6/9, 7/9, as determined by the filling probability of each bucket relative to a given reference bucket.

The tallest peak in the MCA spectrum corresponds to the detection of pulses by both the CMAs simultaneously (within ~10 ns), where, for example, CMA 1 and CMA2 are looking at the incident core photoelectron and the subsequent Auger decay electron, respectively. The peak 170.2ns later than this peak corresponds to an electron detected in CMA1 at Δt =0ns and another electron detected in CMA2 170.2ns later. The 170.2ns peak clearly cannot be a coincident event, defined as both electrons arriving within ~10ns of each other; in fact, the time difference between core electron emission and the subsequent Auger electron decay from the same atom is in the fs (famto second) range, as mentioned above. The intensity of the 170.2ns peak is used to quantify the accidental coincidence rate since its filling probability is the same as the 0ns peak

2.6 Coincidence and Accident Events

At 180eV photon energy, the Ag 4p ($N_{2,3}$) photoelectron peak is observed at 133 eV, while the Auger decay of this core level, the Ag $N_{2,3}VV$ Auger peak, is observed at 38 eV. The sequence of events in an Auger-photoelectron coincidence measurement is as follows. First, a bunch of electrons in the ring generates a photon that is incident on the sample and excites the Photoelectrons and the Auger electrons. Consider that CMA1 is set such that it is receiving the 4p core photoelectrons while CMA2 is set to scan over the NVV Auger spectrum. To explain the measurement of true coincident and accidental coincidence events, lets us consider two atoms, labeled A and B. When atom A is excited, an $N_{2,3}A$ electron and an $N_{2,3}VVA$ electron are released. Atom B, on excitation, releases an $N_{2,3}(B)$ photoelectron and an $N_{2,3}VV(B)$ Auger electron. The bunch which excites the atom can be indicated by a subscript to this notation, i.e., if bunch 1 excites atom B and an NVV Auger electron is emitted, this event would be indicated by $N_{2,3}VVB_1$. Since bunch 1 excites both atom A and atom B, the coincidences would be the ones in which the measured electrons originate come from a single atom. Thus, when $N_{2,3}A_1$ is captured by CMA1 and $N_{2,3}VVA_1$ is captured by CMA2, then it's a true coincidence. When CMA1 captures $N_{2,3}VVA_1$ and CMA2 captures $N_{2,3}B_1$, then it's not a coincidence and is an accidental event, as

the two electrons came from two different atoms. So even these accidents are seen at **Δ**t =0 (i.e. ROI 0) along with the coincidence events.

The next peak after **Δ**t =0 arises from electrons arriving at CMA2 one bunch later than **Δ**t =0, i.e. at **Δ**t =18.9ns. Since this timing difference is much greater than the ~fs time between photoelectron and Auger emission from a single site excitation, only accidental coincidence events contribute to this peak. The accidental rate here is smaller than the accidental rate in the **Δ**t =0 time peak, as described above.

Two regions of interest are selected corresponding to the **Δ**t =0 and **Δ**t =170.2ns between singles events, and named ROI 0 and ROI 1, respectively. They are indicated as regions C and A, respectively, in Figure 2.8. When the timing pulse height is within ROI0 or ROI1, the MCA send a TTL output pulse to the Coincident or Accident output channels, respectively. A convenient way to set ROI 0 and ROI 1 is with the incident flux is turned way up, causing the MCA spectrum to build up quickly, with good statistics, making it easy to determine the minimum and maximum end of these ROIs. At this large flux, the True to Accident coincidence ratio (T/A) would go to nearly zero, which is not a good way to collect coincidence data. Therefore, under actual data collection conditions, the incident flux is reduced until T/A is in the 0.2-0.5 range.

The time interval between excitation and detection in a CMA depends upon two factors: 1) Electron kinetic energy and 2) Pass energy of the analyzer. The first factor applies to the relatively short flight path from the sample to the CMA entrance mesh, while the second factor applies to the much longer flight path, at the pass energy, through the CMA. Every time the either of these energies is changed, the timing windows of the MCA need to be adjusted. We do not vary the CMA pass energy during an APECS scan, but we necessarily change the kinetic energy in order to scan the desired range of the photoelectron or Auger spectrum. If this energy range is large enough, the timing windows also need to be adjusted during each spectral sweep. For the APECS spectra shown in this thesis, the range of kinetic energy scanned is 10-85eV, encompassing the entire Low Energy Tail (LET) and the $N_{2,3}VV$ Auger peak. This range, more than a factor of 8, certainly requires adjustment of the ROIs during each sweep. We selected

three kinetic energy ranges to cover this range: 10-25 eV, 25-45 eV, 45-85 eV. The shift of the ROIs within each of these three ranges is small enough to be neglected.

Table 2.1 ROI selected for different Electron Kinetic Energy ranges

Electron Kinetic Energy (eV)	ROI (0)	ROI (1)
10 – 25 eV	255 – 310	699 – 754
25 – 45 eV	268 – 323	711 – 766
45 – 85 eV	276 – 331	719 – 774

CHAPTER 3

EXPERIMENTAL CONSIDERATIONS AND PROCEDURE

We study the correlation between the subsequently emitted electrons from a solid after photo-excitation. Different techniques like Photoelectron and Auger electron Spectroscopy have been successfully used in the study of the electron structure in solids. The spectrum obtained using these techniques can provide us with specific information about the core electrons and the valence band electron structure. Lifetimes of Auger decay are of the order of 10^{-15} seconds, while the laboratory timing resolution is of the order 10^{-9} seconds for electronic events. Photoelectron and the corresponding Auger electron thus appear to be received at the detector simultaneously. Two electron analyzers are used in Electron-Electron Coincidence Spectroscopy (EECS). In Auger Photoelectron Coincidence Spectroscopy (APECS), which is a type of EECS, one of the analyzers detects the higher energy photoelectron emitted, while another analyzer is tuned to scans the lower energy Auger electron spectrum. On detection of electrons in both the analyzers simultaneously, in the experimental time resolution, it is inferred that both the electrons detected belong to the same atom and the same excitation event. An Auger spectrum (referred to here as the Singles spectrum) is also acquired during the experiment and is not based on the coincidence technique as both the electron analyzers are scanned over the same energy range.

For the coincidence experiment, we aim to generate high energy resolution data in short amount of time. To obtain good statistics, increasing the incident photon energy flux does not have a significant reduction in the time required to obtain desired level of data. Thus the increase in energy can not make up for the counts reduced due to coincidence experiment, making the experiment setting apparatus design critical. The following chapter discusses the experiment results.

The sample used in the APECS experiment is a single crystal specimen of 10 mm in diameter and 3 mm thick. The sample was sputtered and annealed periodically using the below stated procedure. Once the sample is cleaned, a wide range photo-electron energy spectrum was acquired at 180 eV incident photon energy. As seen in the Figure 1.3, the spectrum consists of photo-electrons (from both core and valence bands) and Auger electron (NVV) peaks. When photo-electron spectra are taken at different incident photon energies, the change in the position of the photo-electron peaks can be noted. The Auger electron peaks do not change their position in the spectra as the Auger electron energy is independent of the incident photon energy.

The contribution to the low energy tail and the Auger peak, as seen in the singles spectrum, due to events other than the core photo-electron emission event, can be eliminated by using the coincidence technique.

3.1 EECS Experiment

The experiments were performed at the beamline U1A at the National Synchrotron Light Source (NSLS) at Brookhaven National Lab, which was described in the previous chapter is used for the APECS measurements. The computer controlled power supplies and the timing electronics are used to detect the timing interval between the electrons detected by the two CMAs. These readings give rise to three spectra, viz. the singles spectra, the total coincidence spectra which includes true and accident coincidences. To generate the true coincidence spectrum, we subtract the accidental contribution from the total coincidence spectrum.

One of the CMAs is scanned over the spectrum of interest in the coincidence measurements. The CMA is operated with a large aperture (1.6% (KE)/KE) and the pass energy is set to 80 eV. The larger apertures help in maintaining the true coincidence rate and the true to accident ratio at an acceptable level.

3.2 Sputtering and Annealing

The Ag sample is sputtered alternate days with Ar^+ ion bombardment for 20 minutes. And annealed at 300º C for about 100s by radiative heating from a nearby W filament. The filament current was set to 20 A.

3.3 APECS Experiment: NVV Auger in coincidence with the N core photo-electrons

The sample is placed in the endstation UHV chamber. Photons of appropriate energy are made incident on the sample where they excite Photoelectrons, Auger electrons, and other secondary electrons from the sample surface. The two Cylindrical Mirror Analyzers (CMA 1 and CMA 2) are maintained at the energies of the Photoelectron decay peak and the subsequently emitted Auger electron peak respectively. They capture the electrons emitted from the sample. The CMA1 is fixed at the photoelectron energy, while the CMA2 scans over the energy range that includes the Auger electron peak. Both the electrons are assumed to be reaching the CMAs simultaneously, as the time difference between them is only about 10 femtoseconds, which is very less than the timing resolution of the CMAs (~ 10^{-9} sec).

Synchrotron radiation of energy hv (180 eV) is made incident in the sample. It photo-excites from the atomic core level with binding energy E_C. The photo-excited electron now exits the sample and gets detected by the CMA analyzer. Due to this excitation, the core hole is left in the solid and an excited ion results. This ion can be stabilized by two possible processes: X-ray fluorescence and Auger electron emission. For core holes with binding energy less than 2 keV, the preferred method of stabilization is Auger electron emission. [12]

As shown in the Auger process in Figure 1.1 the excited ionic system is relaxes via a process in which electron from the Valence band loses energy to fill the core hole created in the N (4p) core shell during the photo-excitation process. A second electron is then emitted out from the valence band of the atom for energy conservation and is termed as the NVV Auger electron. In this type of CVV Auger transition, the final state consists of two holes in the valence band.

In our measurements, photon energy of 180 eV was selected in order to emphasize 4p core electron production, which has a binding energy of 133 eV. The right-hand CMA was fixed at the energy of the 4p core peak, 133 eV. The left-hand CMA was scanned for the NVV Auger peak between 10 to 85 eV. The coincidence experiment takes a considerably long time to get good statistics. Therefore, we take proper care that we do not lose the entire acquired data even if

some technical problem is faced during a small time period during the experiment. To achieve this the scans have been saved each time after 30 sweeps are completed. After saving all the scans for the entire experiment period, the scans are added together.

3.4 LET in coincidence with the Inelastically scattered Valence Photo-electrons

The APECS spectrum contains background due to true coincidence between photo-emitted valence band electrons that undergo inelastic scattering. These electrons transfer part of their energy with other valence electrons which exit the sample. Inelastically scattered photo-electrons can be observed as background exclusively in between the 4p core photoelectron peak at 133 eV and the valence band peaks at about 186.7 eV. This background extends further till low energy in the spectrum. It is not observed as other peaks and their backgrounds sit over it. The 4p core photoelectron peak too sits on this background. Therefore, in the experiment explained previously in Section 3.3, the LET consists of not only the inelastically scattered 4p photo-electrons, but also the inelastically scattered valence photo-electrons. The measured Ag 4p NVV LET contains a significant fraction of LET emission coincident with the background emission at the Ag 4p photo-electron kinetic energy, but unrelated to the Ag 4p excitation event. It's important to separate the Ag 4p NVV APECS LET from this background LET, leaving the pure Ag LET spectrum created by excitation of Ag 4p photoelectrons only. This separation cannot be accomplished via APECS, since the fixed channel contains indistinguishable contributions from Ag 4p photo-electrons and inelastically scattered background emission.

A series of APECS measurements made with the fixed analyzer set at energies 150 eV, 160 eV, 171.5 eV, 175 eV and 186.7 eV, which are above the 4p core photoelectron peak were used to obtain and estimate this background. Here the final value, 186.7 eV is in the middle of the Ag valence band. The right-hand CMA was fixed at these energies of the inelastically scattered valence photo-electrons. The left-hand CMA scans the LET region between 10 to 85 eV.

From Chapter 1 (Eq. 4), we have

$$\Delta = h\nu - E_{V1} - KE_{InelasticValance1} - \phi_A \quad (1)$$

Where, $KE_{InelasticValance1}$ represents the energies at which the fixed analyzer is set, i.e., 150 eV, 160 eV, 171.5 eV, 175 eV and 186.7 eV.

hv = Incident photon energy (plus a -15 V Sample Bias)

E_{V1} = Binding Energy of the outgoing valance electron (~0 eV in case of Ag Fermi level electrons

ϕ_A = Work function of the analyzer (~4.5 eV for the CMAs)

Based on the equation (1) above Table 3.1 gives the Δ values for the various Fixed analyzer energies.

Table 3.1 Fixed Analyzer Energies with their corresponding Δ values

Fixed Analyzer Energies (eV)	Δ(eV)
133 eV	57.5 eV
150 eV	40.5 eV
160 eV	30.5 eV
171.5 eV	19 eV
175 eV	15.5 eV
186.7	~ 0 eV

Now, from Equation 5 in Chapter 1, the electron that accepts this energy Δ is inelastically emitted with an energy given by,

$$KE_{InelasticValance\ 2} \leq \Delta - E_{V1} - \phi_A \qquad (2)$$

This is the threshold value below which the contribution of the inelastically scattered valence band electron would be observed at the various Fixed Analyzer energies. The $KE_{InelasticValence\ 2}$ values for various Fixed Analyzer energy values are calculated using Equation 2 above and tabulated below.

Table 3.2 Energy of the Inelastically Scattered Valence band Photo-electrons

Fixed Analyzer Energies (eV)	KE $_{\text{Inelastic Valence 2}}$
133 eV	≤ 53 eV
150 eV	≤ 36 eV
160 eV	≤ 26 eV
171.5 eV	≤ 14.5 eV
175 eV	≤ 11 eV
186.7	~ 0 eV

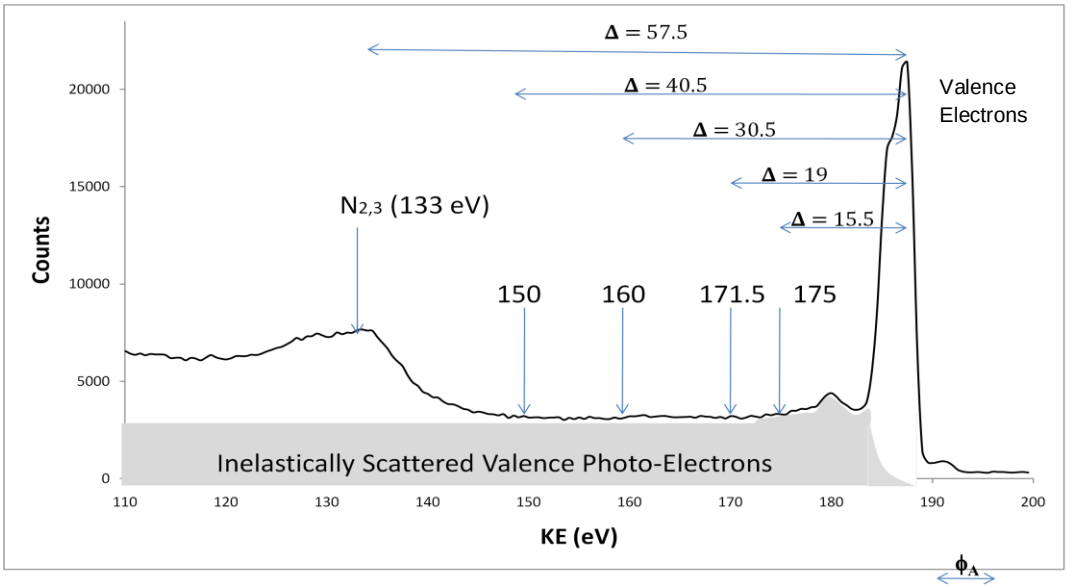

Figure 3.1 Ag Photoelectrons spectrum at hν= 180 eV and a (-15 V) sample bias. The various fixed analyzer positions along with the respective **Δ** values are indicated

CHAPTER 4

EXPERIMENTAL DATA AND DISCUSSION

4.1 Ag Photoelectron Spectrum at hν = 180 eV

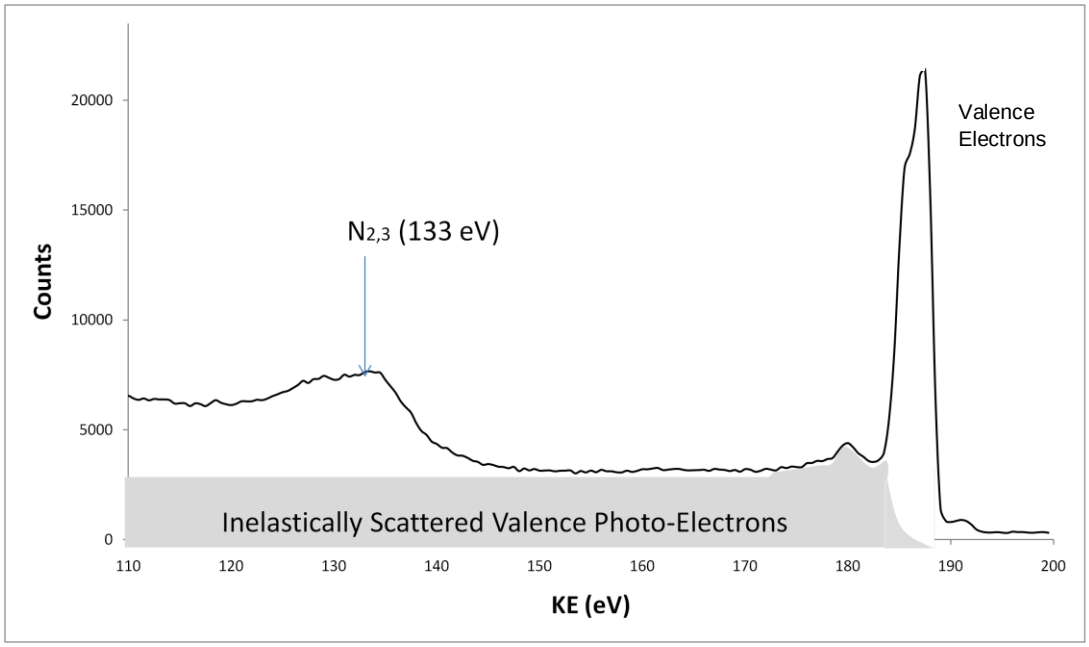

Figure 4.1 Ag (100) Photoelectron spectrum taken at hν =180 eV and a (-15 V) sample bias.The shaded portion indicated contribution to the spectrum due to inelastically scattered valence band photo-electrons

4.2 Ag 4p NVV APECS Spectrum

At 180eV photon energy, the Ag 4p photoelectron peak is seen at 133 eV. We measured the Ag 4p NVV APECS LET spectrum at this fixed energy and at a few kinetic energy values higher than 133eV, up to the valence band seen at 186.5 eV electron kinetic energy. We chose to measure background APECS LET spectra at the following fixed analyzer kinetic energy values: 150, 160, 171.5, 175 and 186.5 eV, where the final value is in the middle of the Ag valence band.

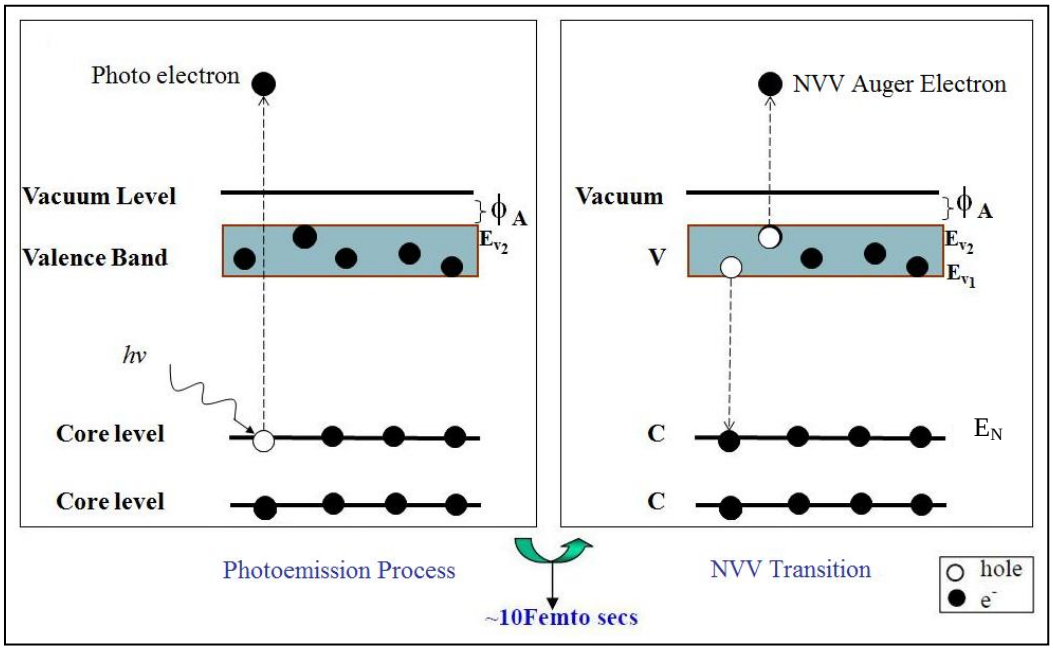

Figure 4.2 NVV Auger Decay

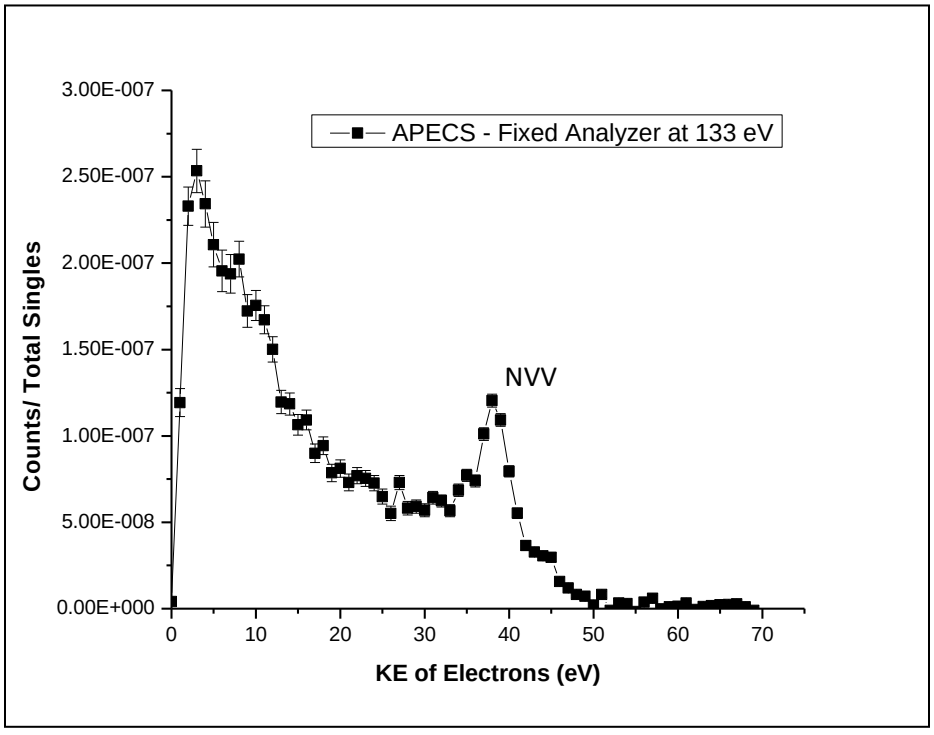

Figure 4.3 RH-CMA Fixed at 133 eV [The Ag 4p NVV APECS Spectrum]

4.3 Ag APECS 4p NVV spectrum in comparison with the Photo-electron spectrum

It is evident from the singles and the coincidence spectra that the use of the coincidence spectroscopy successfully eliminates the background of the inelastically scattered electrons and other secondary electrons.

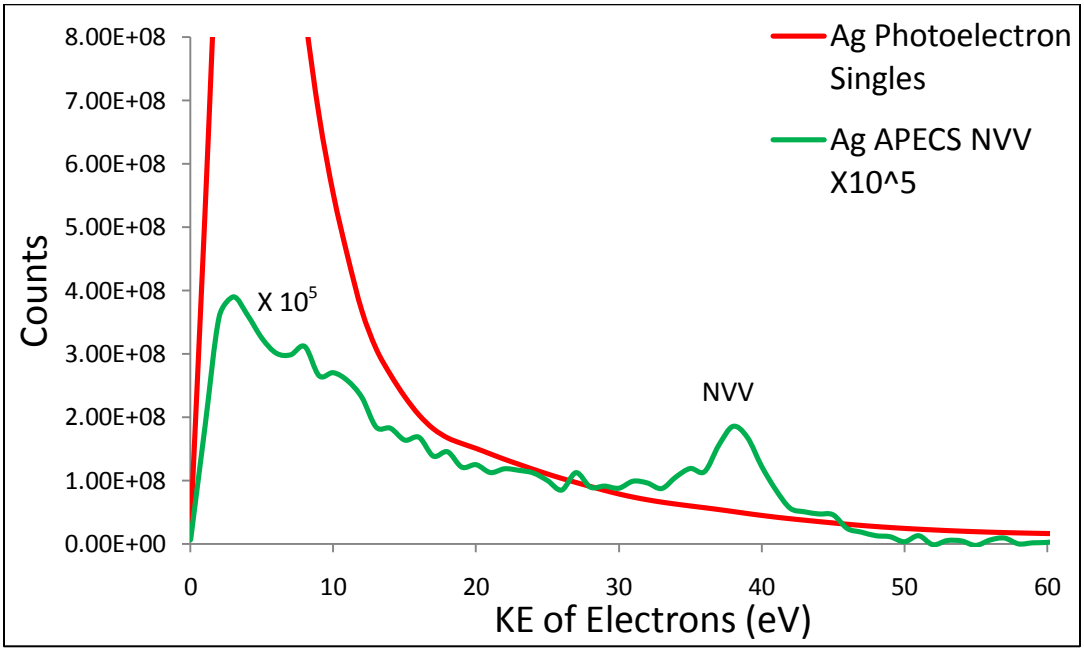

Figure 4.4 Ag APECS 4p NVV spectrum in comparison with the Photo-electron spectrum

We have estimated the contribution to the LET due to processes extrinsic to Auger transitions in APECS technique. if the fixed energy analyzer is set to the Ag 4p core photo-electron peak, the APECS LET contains only decay features of that core excitation process, i.e. Auger emission peaks and inelastically scattered 4p electrons. In this way, the Ag 4p NVV APECS spectrum reveals the Ag NVV Auger peak which is swamped by secondary electron emission in the non-coincidence LET spectrum. In practice, the Ag 4p photo-electron peak sits on top of LET emission from higher kinetic energy photoemission or Auger emission peaks.

4.4 Inelastic Scattering of Valence level Photo-Electrons

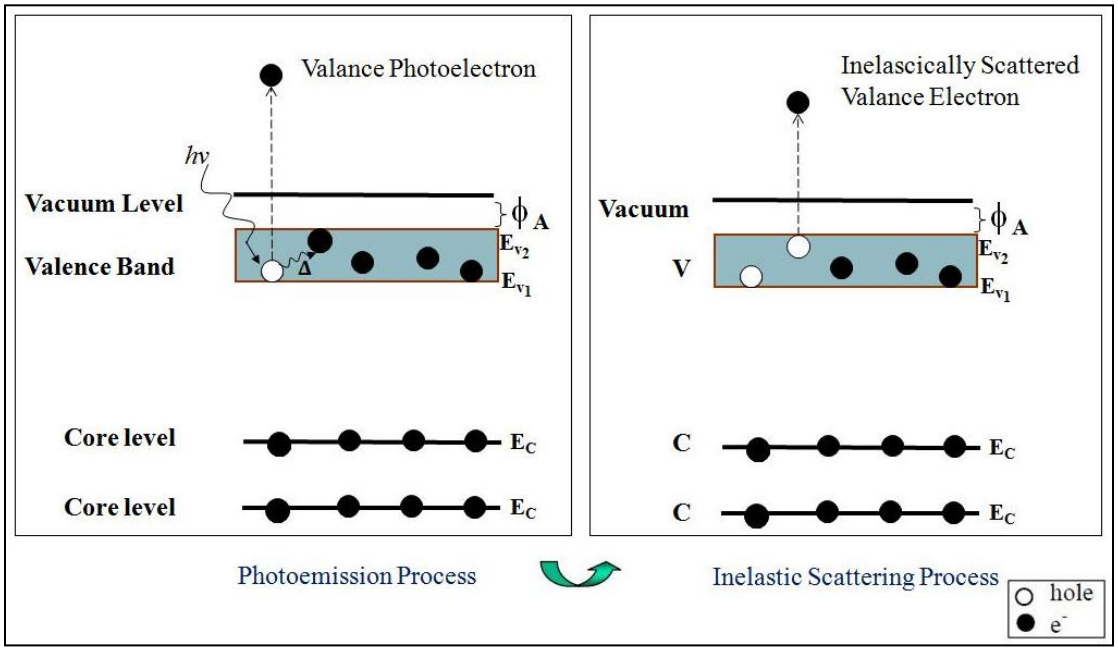

Figure 4.5 The Inelastic Scattering of Valence level Photo-Electrons

In an event of inelastic scattering of this outgoing photo-emitted valance band electron, it transfers an energy **Δ** is transferred to another neighboring valance band electron. Thus, now it gets emitted with an energy reduced by a value of Δ and is given by equation (4) in Chapter 1.

Inelastic scattering event of photo-emitted valance band electrons is as seen in the Figure 4.5.

For the Conservation of Energy principle to be satisfied, in this inelastic scattering event the other valance electron which accepts energy ≤ **Δ** eV from the photo-emitted valence electron and leaves the atom with a kinetic energy given by the equation (5) in Chapter 1.

4.4.1 LET in coincidence with the Inelastically scattered electrons at 150 eV

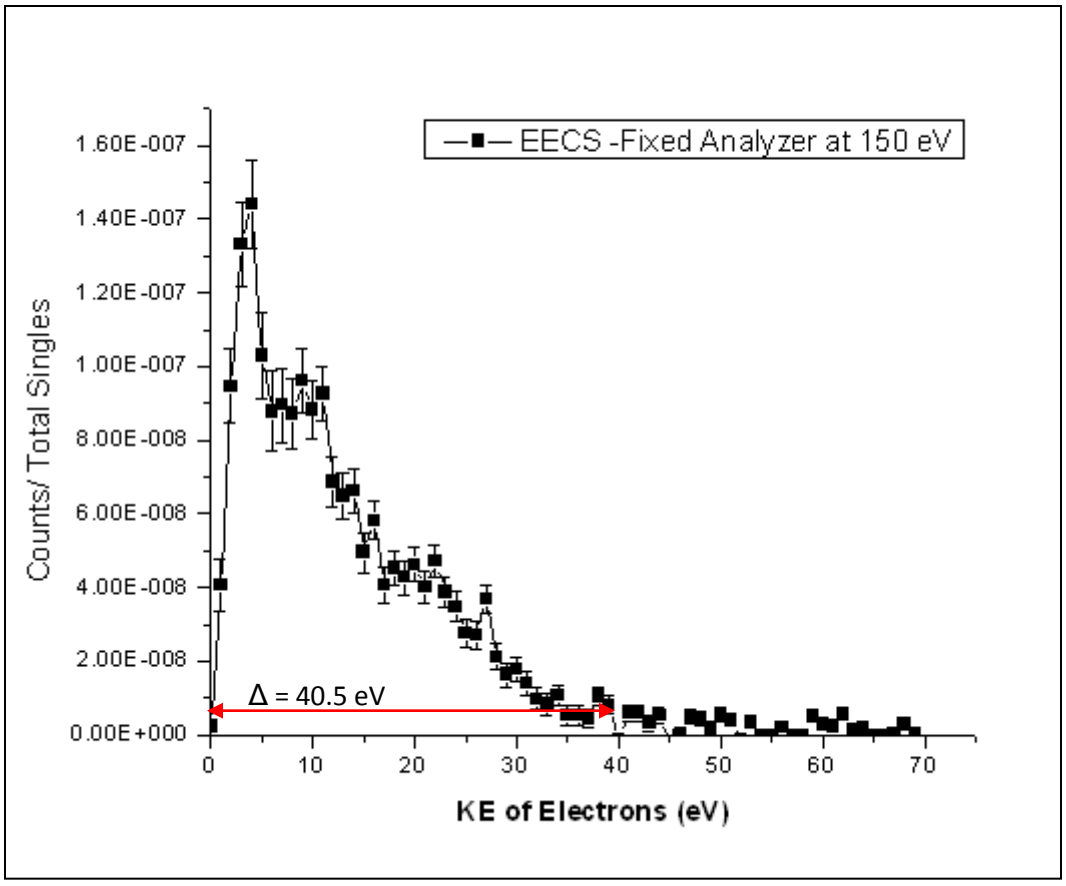

Figure 4.6 EECS spectrum with Fixed Analyzer set at 150 eV electron energy

The spectra have been shifted by 15 eV to account for the -15 V sample bias. The horizontal axis represents the Kinetic Energy of the electrons as they leave the sample surface. The photon energy $h\nu$ = 180 eV.

4.4.2 LET in coincidence with the Inelastically scattered electrons at 160 eV

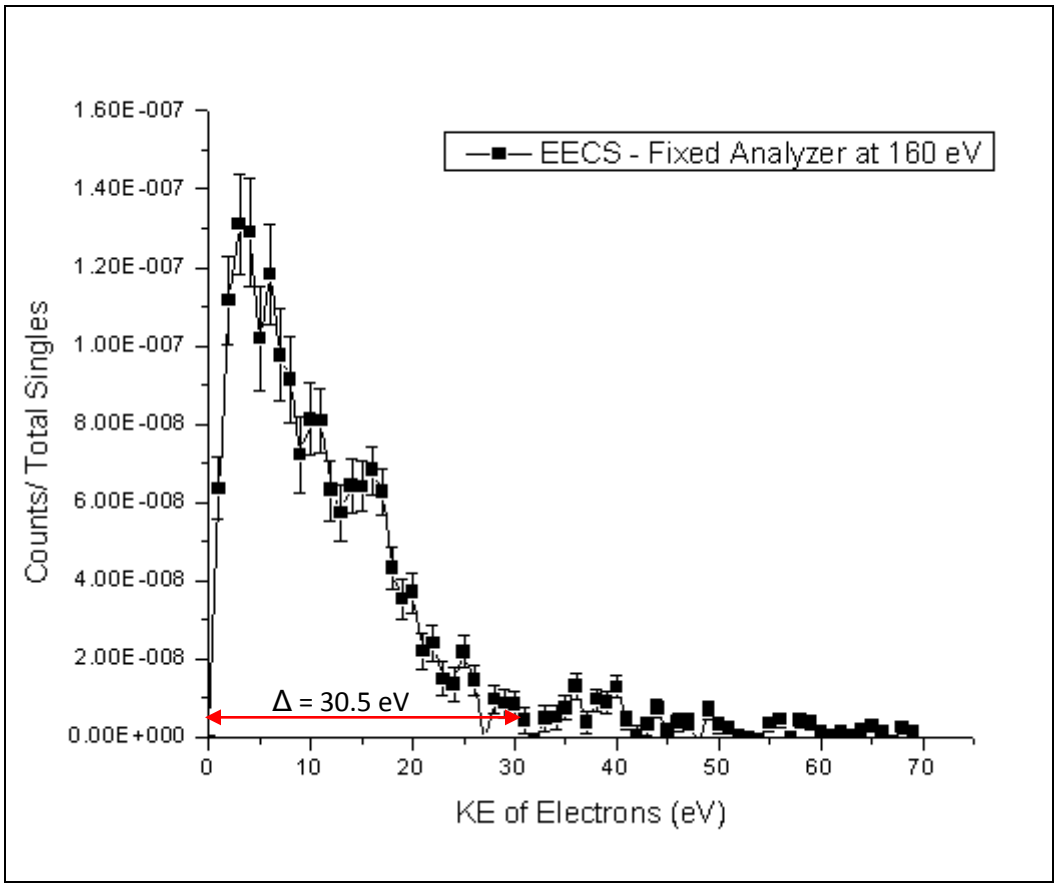

Figure 4.7 EECS spectrum with Fixed Analyzer set at 160 eV electron energy

The spectra have been shifted by 15 eV to account for the -15 V sample bias. The horizontal axis represents the Kinetic Energy of the electrons as they leave the sample surface. The photon energy $h\nu$ = 180 eV.

4.4.3 LET in coincidence with the Inelastically scattered electrons at 171.5 eV

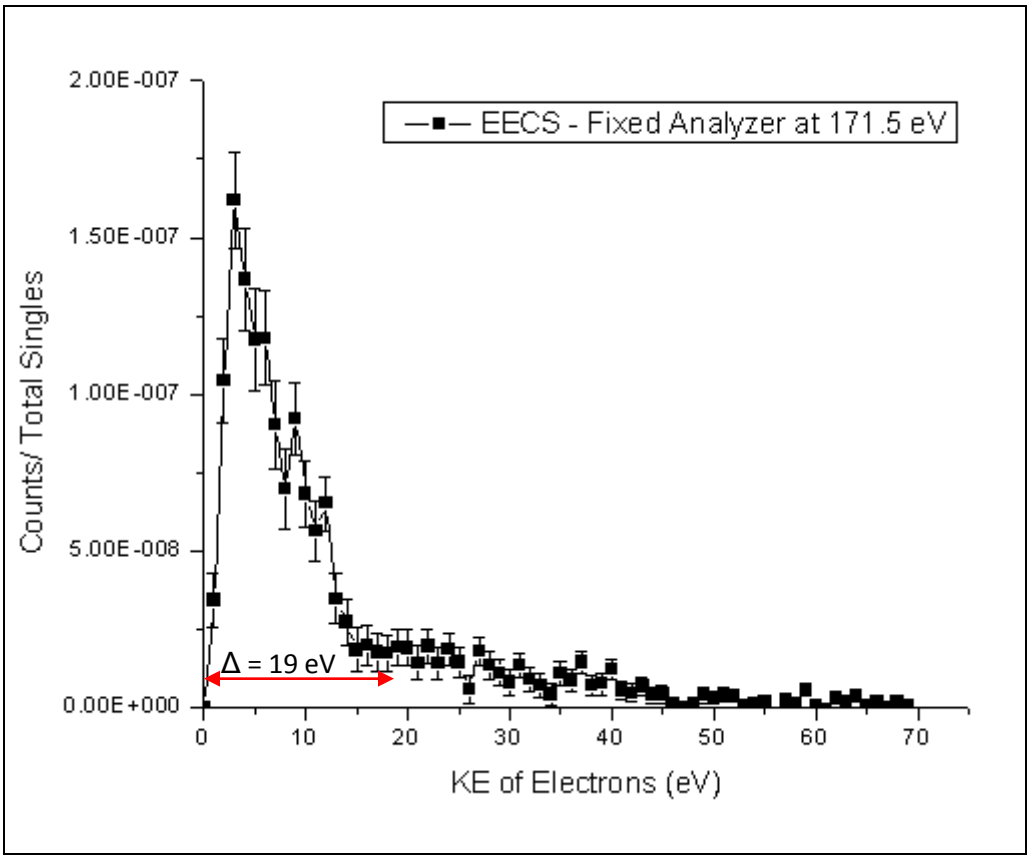

Figure 4.8 EECS spectrum with Fixed Analyzer set at 171.5 eV electron energy

The spectra have been shifted by 15 eV to account for the -15 V sample bias. The horizontal axis represents the Kinetic Energy of the electrons as they leave the sample surface. The photon energy $h\nu$ = 180 eV.

4.4.4 LET in coincidence with the Inelastically scattered electrons at 175 eV

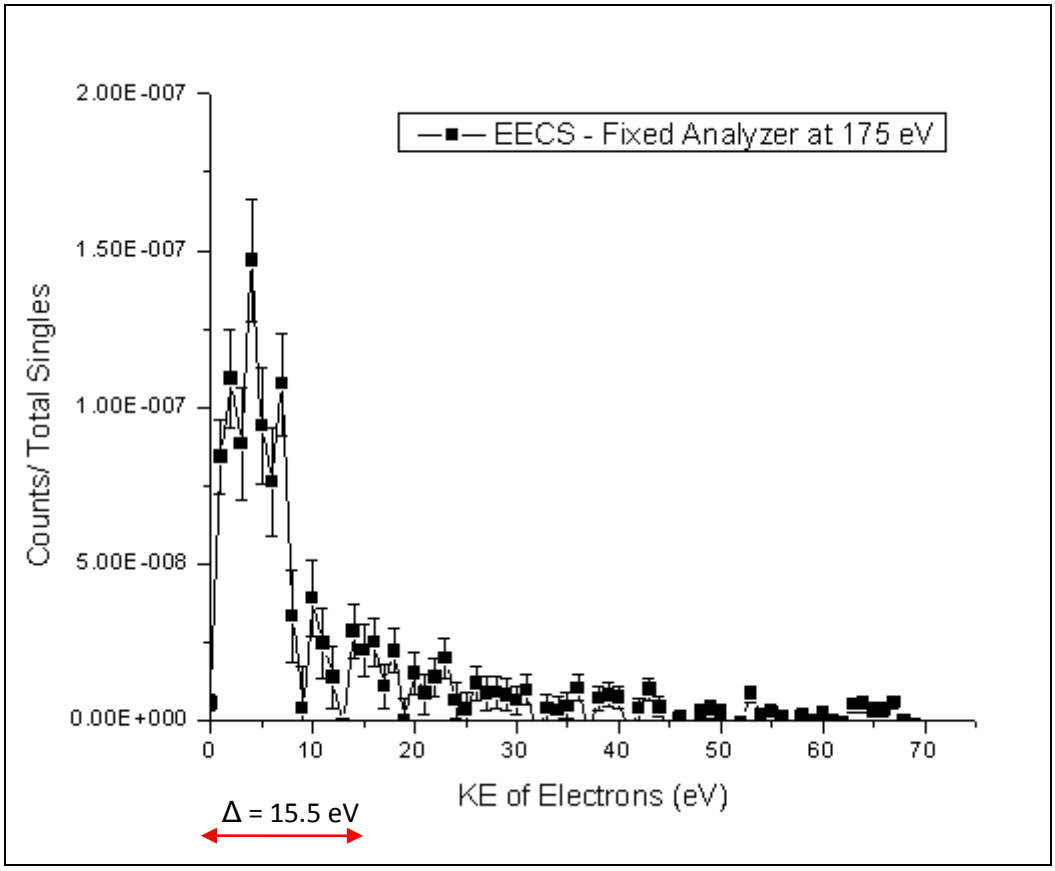

Figure 4.9 EECS spectrum with Fixed Analyzer set at 175 eV electron energy

The spectra have been shifted by 15 eV to account for the -15 V sample bias. The horizontal axis represents the Kinetic Energy of the electrons as they leave the sample surface.The photon energy $h\nu$ = 180 eV.

4.4.5 LET in coincidence with the Inelastically scattered electrons at the center of the observed valance electron peak energy (186.7 eV)

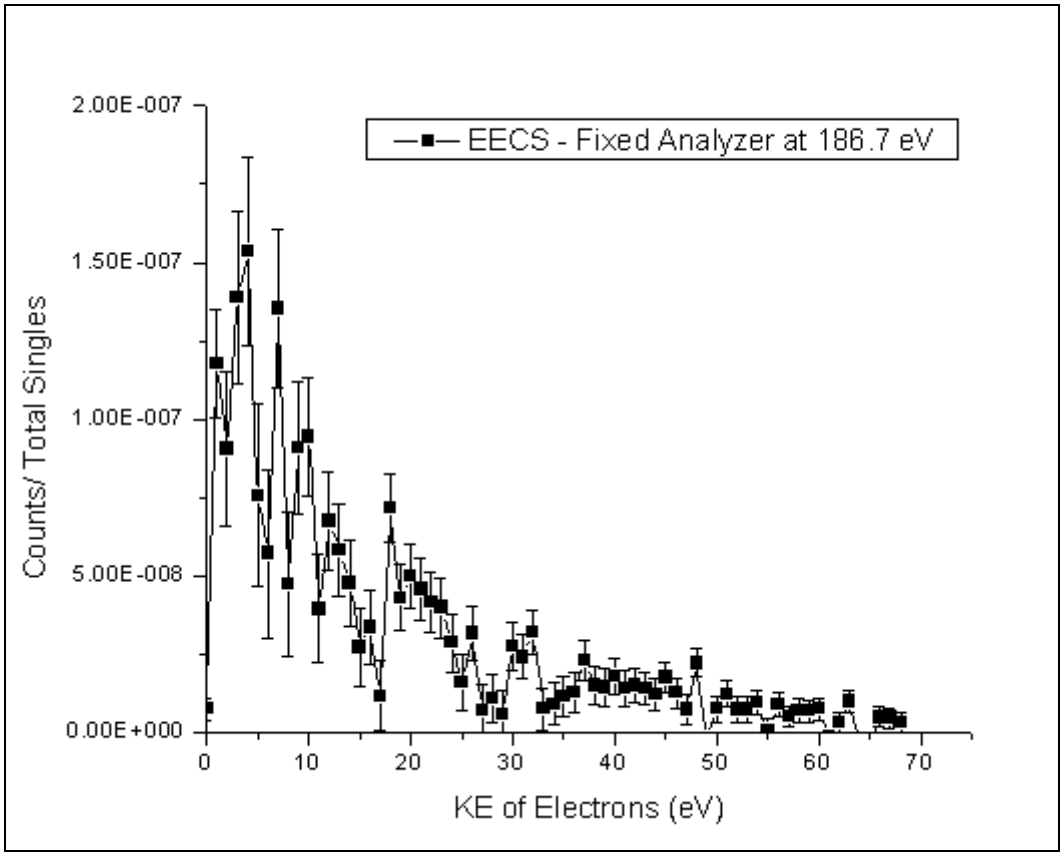

Figure 4.10 EECS spectrum with Fixed Analyzer set at 186.7 eV electron energy

The spectra have been shifted by 15 eV to account for the -15 V sample bias. The horizontal axis represents the Kinetic Energy of the electrons as they leave the sample surface. The photon energy $h\nu$ = 180 eV.

4.4.6 Overlap of the spectra obtained at various Fixed Analyzer energies

This overlap only occurs when the spectra are normalized to the total singles.

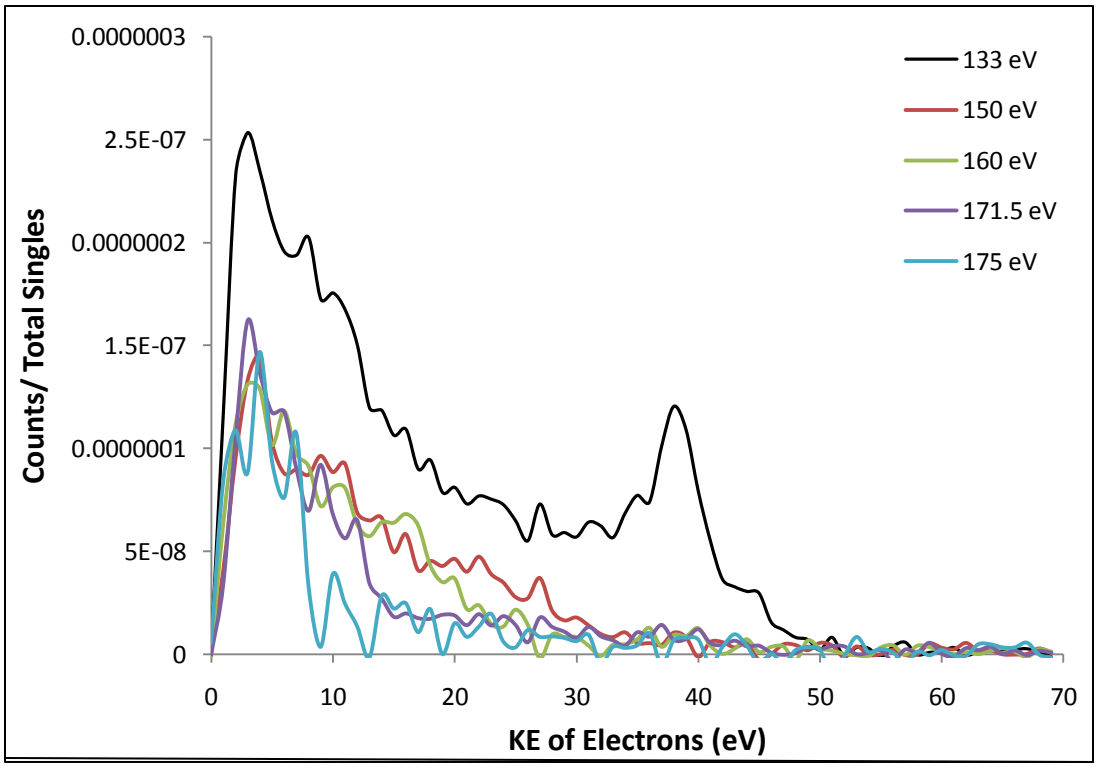

Figure 4.11 Plot showing the overlap of the APECS spectrum at 133 eV Fixed analyzer energy and the EECS spectra at fixed analyzer energies of 150, 160, 171.5, 175 eV

The spectra have been shifted by 15 eV to account for the -15 V sample bias. The horizontal axis represents the Kinetic Energy of the electrons as they leave the sample surface. The photon energy $h\nu$ = 180 eV.

Here we observe that the background spectra follow a trend by falling in an order one after the other in the low kinetic energy range. This trend is seen to be followed upto a specific x-axis KE value where the spectra drop to zero counts. The spectrum for 186.7 eV fixed analyzer energy is not included in this overlap for reasons discussed in the next section.

4.5 Discussion

The trend visible in the background spectra is that they all fall in an order one after the other, at low KE, up to a value that depends on the value of the fixed KE, given approx. by the expression [195eV – (fixed KE value) – E_{v1} – ϕ_A], at which point they all drop to approximately zero counts. (See Table 3.1) Here, 195 eV is the photon energy incident on the sample (180 eV) plus the Sample bias (-15 eV).

One exception to the trend described above is that the APECS LET spectrum for 186.7 eV fixed KE, i.e. the Ag VB energy, doesn't show the threshold and its magnitude at low KE matches that of the other background spectra. The reason that this seems odd is that if the trend described above is real, the threshold for 186.7eV fixed KE should be at ~13eV, which is below the onset threshold for these spectra (determined by the 15V bias), and hence the entire spectrum above this should be approximately zero.

A possible explanation for the relatively large signal observed in the coincidence measurements made with the fixed analyzer set at the VB peak can be found in the fact that the VB peak is ~5 times higher than the LET associated with the VB peak. The true coincidence rate is proportional to the joint probability of a photon resulting in a detected electron in both the fixed and scanned analyzer simultaneously. Consequently, it should be expected that true coincidences with the VB peak should be ~5 times larger than true coincidences with the LET of the VB peak, everything else being equal. Dividing the results taken with the fixed analyzer set at the VB peak shown in Figure 4.10 a factor of 5 would result in an integrated intensity that is ~10 lower than those shown in Figure 4.11 (obtained at fixed analyzer energies of 133 eV, 150eV, 160eV, and 171.5, eV and 175 eV). However, the fact that the spectra taken in coincidence with the VB peak, was, (while small after normalizing by the relative VB peak height), not statistically equal to zero is still not fully understood at this time given that accidental coincidences were subtracted.

4.6 Ramaker Function for Curve Fitting and Extrapolation

D. E. Ramaker worked on extracting Auger line shapes from experimental Auger electron spectrum. [13] His method involved removal of the background after numerically integrating the derivative spectrum. In his work, he presented methods to extract the Auger lineshapes from the experimental data with SO_4^{2-} and PO_4^{3-} samples.

In case of the valence band photo-electron emission process in Ag, the electron on its way out can inelastically transfers energy **Δ** eV to the neighboring electron. When the inelastic electron emission process is triggered by energy **Δ** eV, the background, to the APECS LET spectrum, consists of both the electrons from primary beam energy and also true secondary electrons coming from the sample. The primary electrons are the inelastic valence photoelectrons and those which are emitted by accepting the entire primary beam energy **Δ** eV. The true secondary electrons are those which are emitted by inelastically accepting or mutually sharing this primary beam energy. The secondary electrons thus exit out with energies ranging from 0 to **Δ** eV.

Method was developed by D. E. Ramaker et. al. to remove the background by least-square fitting an appropriate function to the desired range in the Auger spectrum. On the basis of functions described for true secondary and redistributed primary electrons respectively by Seah [14] and Inokuti [15], Ramaker developed an expression for determination of the background function, given by Equation 1 below:

$$B(E) = \frac{A(E)}{(E + \mathrm{E}_0)(E + \phi)^m} + \frac{B \ln[(E_p - E)/E_b]}{[(E_p - E)/E_b]^n} + C \qquad (1)$$

Where A, B and C are determined by an optimal non-linear curve fit to the observed coincidence plots for inelastically scattered valance electrons. Exponential constants m and n are taken to be 2 and 1.8 for Ag based on research by Seah and Ramaker [14] respectively.

Other variables in the equation can be described as follows:

E = Energy of the secondary electron with respect to vacuum level

E_p = Primary beam energy (**Δ** eV)

E_b = Binding energy of the primary electron

E_0 = Energy constant determined based on an optimal least sq. fit to the observed data.

Here the value of Δ can be found from; $\Delta = h\nu - E_{Fixed} - E_B - \phi_A$

We obtained EECS LET plots with the analyzer fixed at various inelastic valance photoelectron kinetic energy values higher than 133 eV 4p photoelectron kinetic energy: 150 eV, 160 eV, 171.5 eV and 175 eV. The measurements were made with intent to determine the trend vs. fixed kinetic energy of these non-APECS LET spectra. From Chapter 1, (Eq. 1 and 2), the fact that energy Δ eV is transferred by Inelastic Scattered photo-emitted electron to one or more valence band electron(s), inspired us to use the Ramaker function for the intended curve-fitting, thus treating using Δ value at the Ep term in the function. Slight changes were made to the Ramaker function for the best fit to the data and following Ramaker-like function was used for curve-fitting.

$$B(E) = \frac{A(E^{1.4})}{(E + \mathrm{D})(E + \phi)^m} + \frac{B \ln[(E_p - E)/E_b]}{[(E_p - E)/E_b]^n} + C \qquad (2)$$

E_0 is also set as a constant 'D' and E is raised to a power of 1.4.The A, B, C and D values for the optimal non-linear curve fit of Ramaker equation to these plots at above mentioned energy values respectively are derived using OriginPro Version 8.1 software. The Ramaker equation is optimally fitted to the LET observed below the Based on these values at different fixed analyzer kinetic energies, the A, B and C values are estimated for 133 eV energy.

4.7 Curve Fitting using the Ramaker Function

4.7.1 RH-CMA Fixed at 150 eV – Ramaker Function Fit

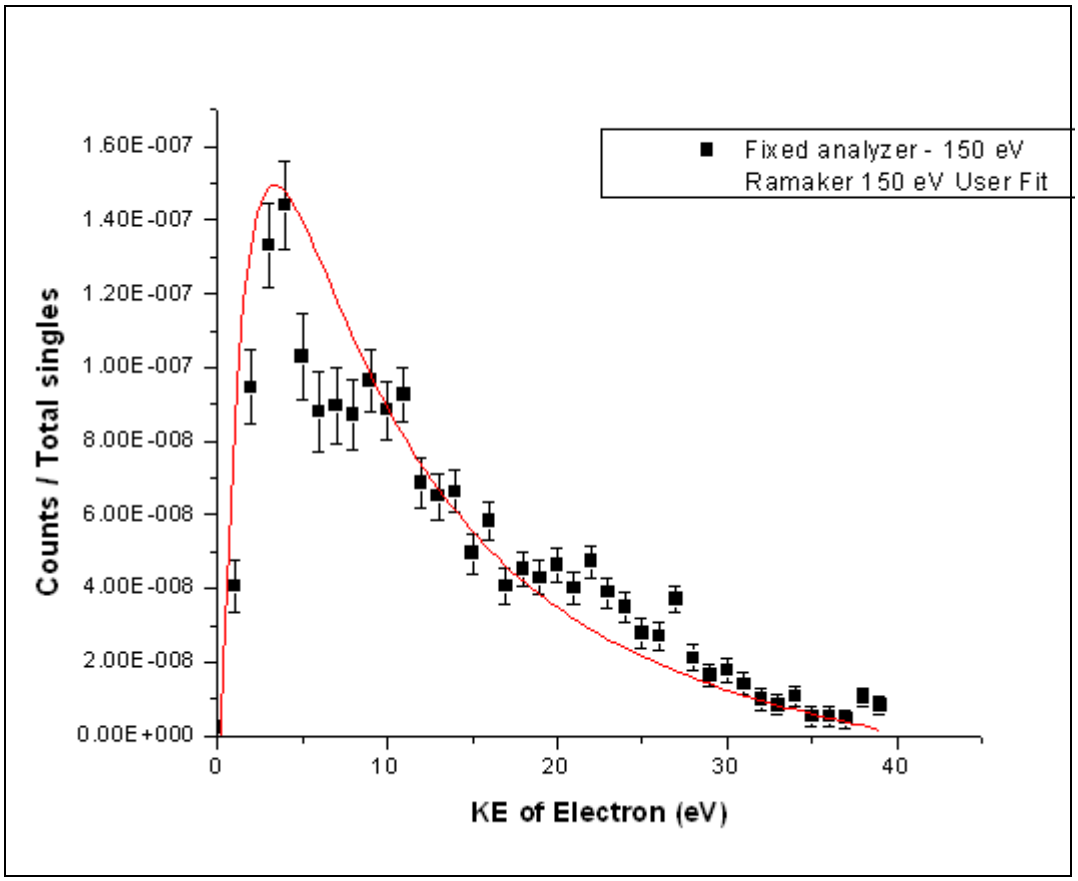

Figure 4.12 Ramaker function fit for EECS spectrum LET with Fixed Analyzer set at 150 eV electron energy

The spectra have been shifted by 15 eV to account for the -15 V sample bias. The horizontal axis represents the Kinetic Energy of the electrons as they leave the sample surface. The photon energy $h\nu$ = 180 eV.

4.7.2 RH-CMA Fixed at 160 eV – Ramaker Function Fit

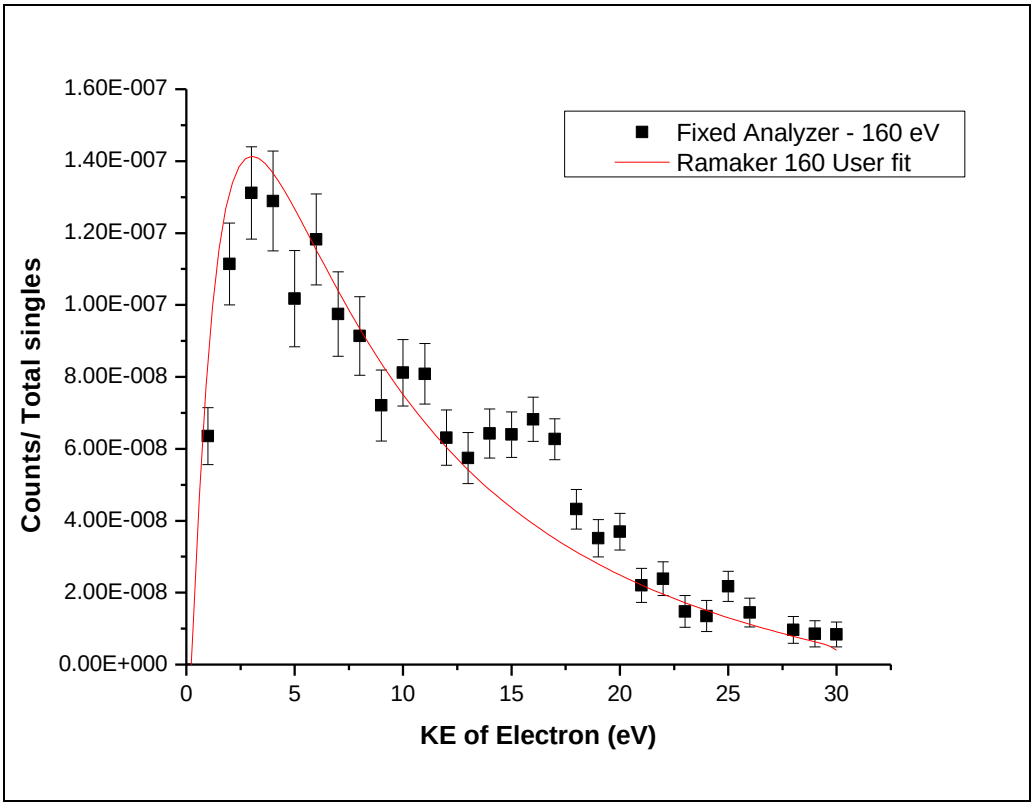

Figure 4.13 Ramaker function fit for EECS spectrum LET with Fixed Analyzer set at 160 eV electron energy

The spectra have been shifted by 15 eV to account for the -15 V sample bias. The horizontal axis represents the Kinetic Energy of the electrons as they leave the sample surface. The photon energy $h\nu$ = 180 eV.

4.7.3 RH-CMA Fixed at 171.5 eV – Ramaker Function Fit

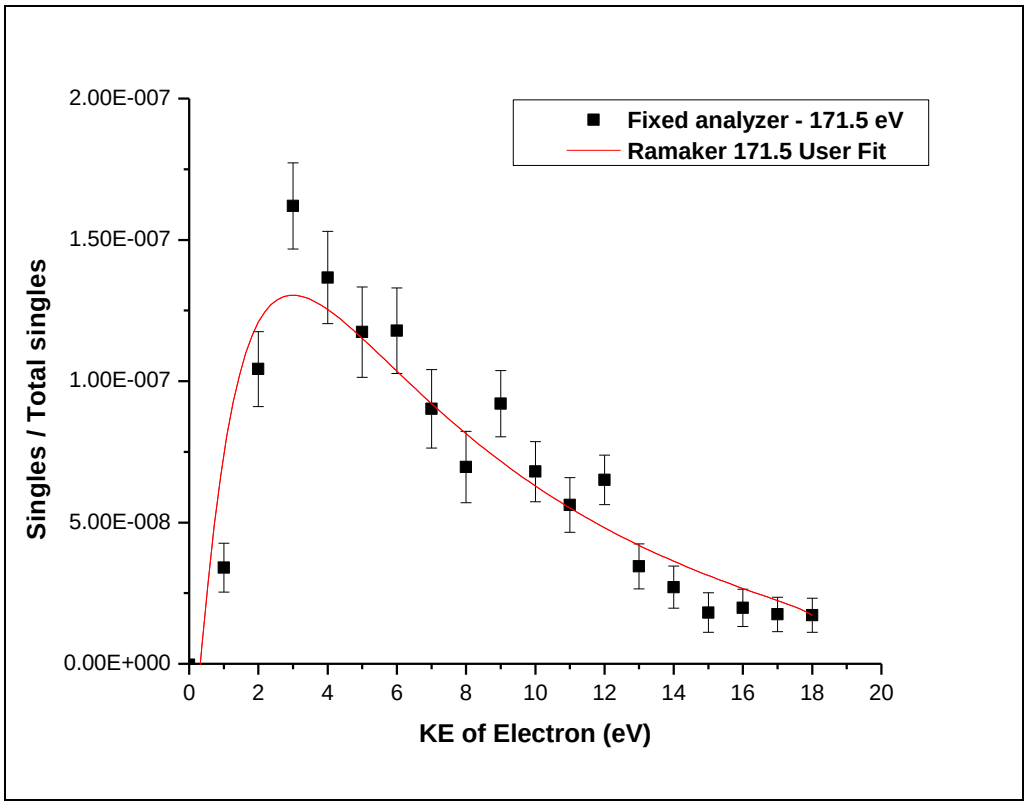

Figure 4.14 Ramaker function fit for EECS spectrum LET with Fixed Analyzer set at 171.5 eV electron energy

The spectra have been shifted by 15 eV to account for the -15 V sample bias. The horizontal axis represents the Kinetic Energy of the electrons as they leave the sample surface. The photon energy $h\nu$ = 180 eV.

4.7.4 RH-CMA Fixed at 175 eV – Ramaker Function Fit

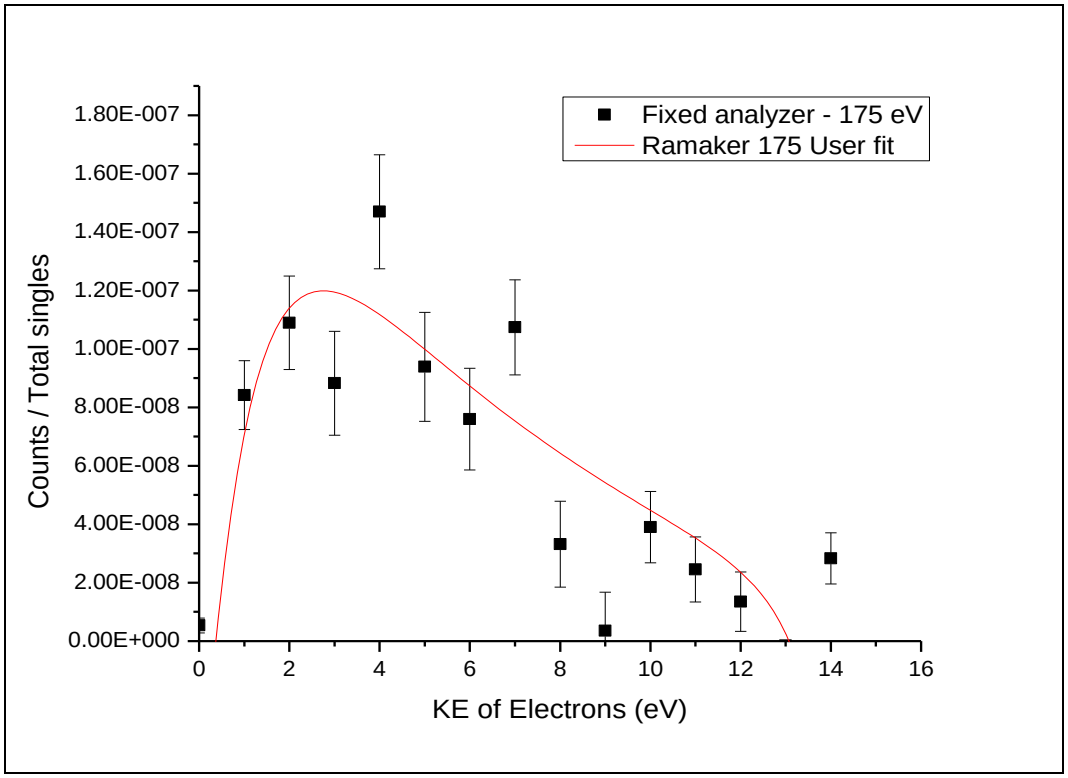

Figure 4.15 Ramaker function fit for EECS spectrum LET with Fixed Analyzer set at 175 eV electron energy

The spectra have been shifted by 15 eV to account for the -15 V sample bias. The horizontal axis represents the Kinetic Energy of the electrons as they leave the sample surface. The photon energy $h\nu$ = 180 eV.

4.7.5 Overlap of the Ramaker Function Curve Fits in comparison with the APECS spectrum

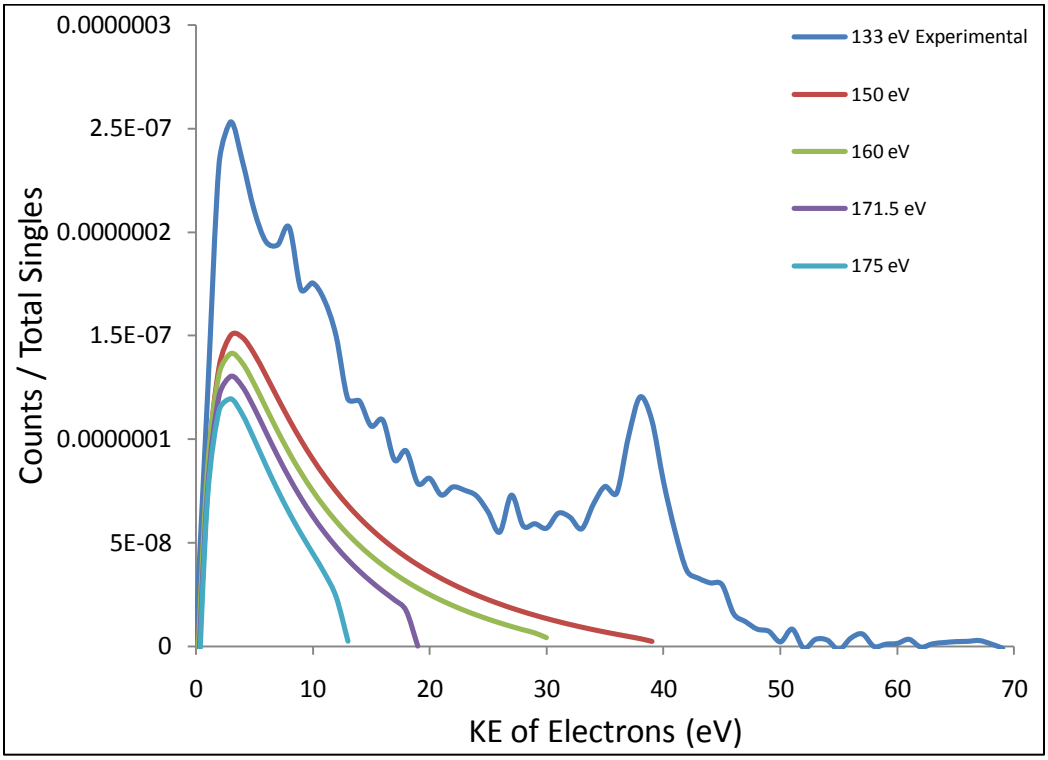

Figure 4.16 Overlap of the APECS spectrum at 133 eV fixed analyzer energy and Ramaker function curve fits for spectra at fixed analyzer energies of 150, 160, 171.5, 175 eV

The spectra have been shifted by 15 eV to account for the -15 V sample bias. The horizontal axis represents the Kinetic Energy of the electrons as they leave the sample surface. The photon energy $h\nu$ = 180 eV.

4.8 Extrapolation using Ramaker Function

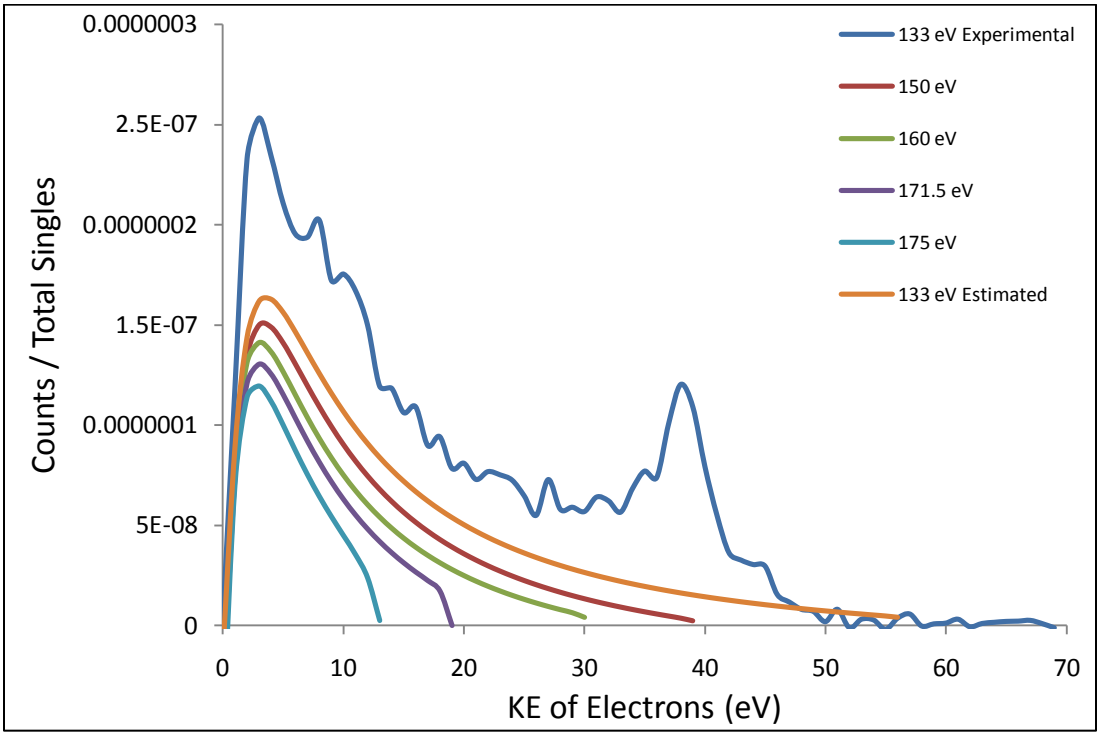

Figure 4.17 Extrapolation for the LET for inelastically scattered valence band photo-electrons emitted at 133 eV

Using the estimated values of the A, B, C and D constants at 133 eV in the Ramaker function, we extrapolate the background curve for the non-APECS LET observed in the APECS LET spectrum [See Appendix D]. The background to the APECS LET is produced mainly due to the inelastically scattered photo-electrons and the multiple low energy electrons emitted by sharing of the photo-electron energy inelastically.

The spectra have been shifted by 15 eV to account for the -15 V sample bias. The horizontal axis represents the Kinetic Energy of the electrons as they leave the sample surface. The photon energy $h\nu$ = 180 eV.

4.9 Background Subtracted APECS spectrum

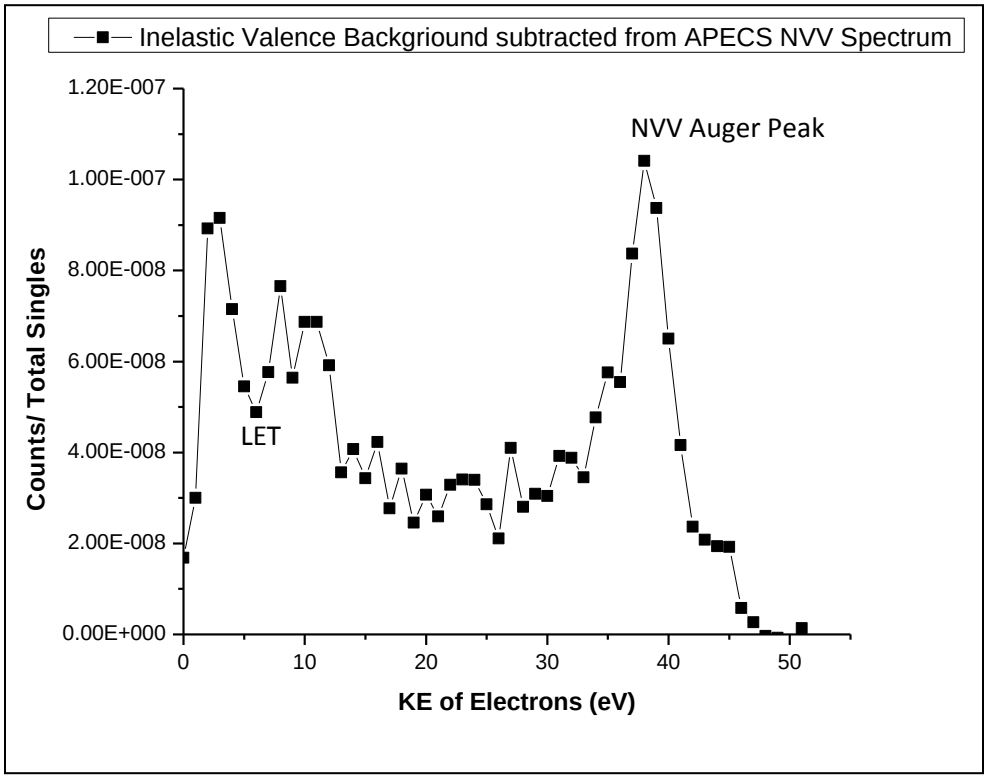

Figure 4.18 The Background subtracted LET for Ag 4p NVV APECS spectrum

On subtraction of this background from the observed APECS data, we get a “pure” Ag LET spectrum created by excitation of Ag 4p photoelectrons only. The reduction in the LET is evident on comparison with the obtained Ag APECS NVV spectrum [See Figure 4.3].

CHAPTER 5

CONCLUSION AND FUTURE WORK

Presented in the thesis are the first-ever measurements of contribution to the APECS spectrum due to inelastically scattered valence band photo-electrons. We used a series of coincidence measurements to obtain spectrum of electrons emitted solely as a result of Auger transitions.

The results presented are consistent with Jensen et. al. [7] hypothesis (based on incomplete measurements). The hypothesis was that the LET is due to electrons emitted at low energies as a result of intrinsic Auger processes.

Also, as mentioned in Section 1.3, we separated the Ag 4p NVV APECS LET from a background due to true coincidence events from inelastically scattered photo-emitted VB electrons. Subtraction of a function derived from a series of auxiliary coincidence measurements allowed us to obtain a “pure” spectrum which is characteristic only to the Auger transitions and provides new data for use in developing algorithm for quantitative analysis of Auger spectrum.

Future work is envisioned in which our experimental data will be applied to study details of the Auger transitions in Cu and other metals.

APPENDIX A

ABBREVIATIONS

UTA	University of Texas at Arlington
BNL	Brookhaven National Libratory
NSLS	National Synchrotron Light Source
IR	Infrared
VUV	Vacuum Ultra Violet
UV	Ultra Violet
AES	Auger Electron Spectroscopy
PES	Photo Electron Spectroscopy
APECS	Auger Photo Electron Coincidence Spectroscopy
SR	Synchrotron Radiation
MCA	Multi Channel Analyzer
PHA	Pulse Height Analyzer
CFD	Constant Fraction Discriminator
CMA	Cylindrical Mirror Analyzer
TAC	Time to Amplitude Converter
ROI	Region Of Interest
LINAC	Linear Accelerator
AMP	Amplifier
ERG	Extended Range Grasshopper
LEBT	Low Energy Beam Transport
XPS	X-Ray Photoelectron Spectroscopy

IC	Inner Cylinder of the CMA
OC	Outer Cylinder of the CMA
KE	Kinetic Energy
VB	Valance Band
D/A	Digital to Analogue
EF	Electric Field

APPENDIX B

EXAMPLE OF APECS NVV SPECTRUM

Wed Sep 1 11:41 2010

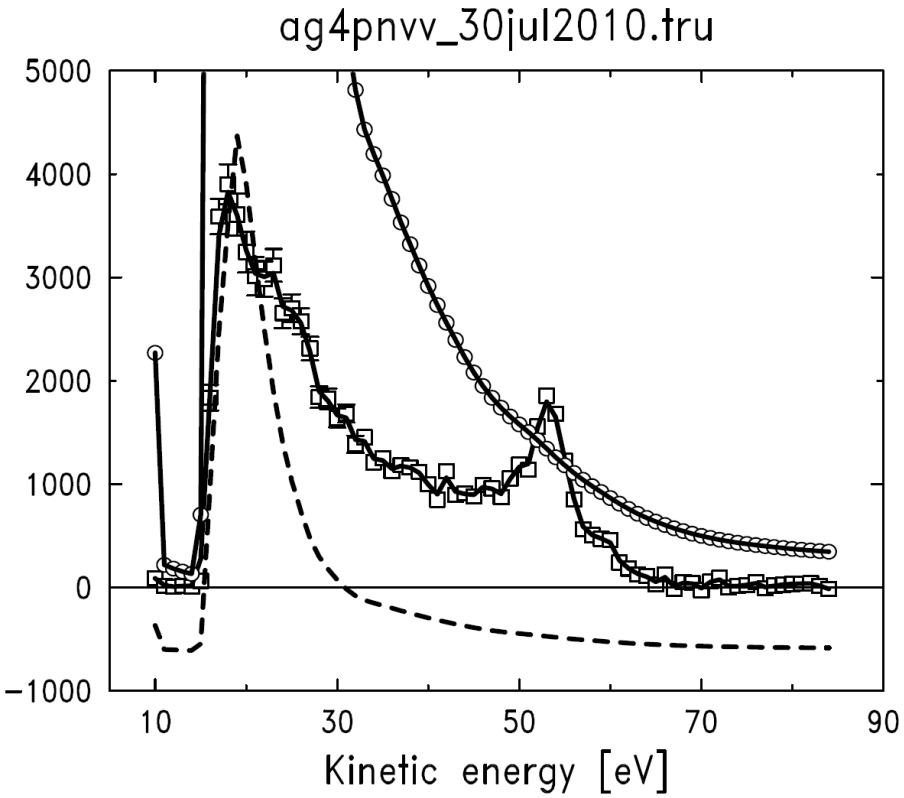

◊ True (raw)
—— True (smooth:1.0eV)
○ s1*K = s1*(Σs2/Σs1)
----- s1 rescaled

χ^2 = 53.177879

K = 2.6532e−05

Iguana sums:

S1 : 1.540e+10
K * S1 : 408711.0
S2 = A : 408711.0
Coi = T+A : 483601.0

T = : 74890.0
T/A = : 0.183235

APPENDIX C

ALGORITHM FOR ADDING ALL SPECTRA

Algorithm For Adding All Spectra [16]

The data acquired in APECS experiments consists of data from singles, coincidence and accidents events. The data obtained is collected in blocks of 30 sweeps each. Thus the block with unforeseen malfunction in some specific part of the experiment can be eliminated later by analyzing the individual files obtained. Elimination of these specific files can avoid loss of a large amount of data. The final spectra are calculated by adding all the individual 30 sweep blocks one by one.

The coincidence data contains the summed coincidence counts, and the corresponding error bars as a function of the kinetic energy of electrons.

The Error Bar = $\sqrt{N}$

Here, N is the number of all coincidence counts at a given energy.

Similarly, the Singles and Accidents data consists of the summed singles and accidents counts as a function of energy respectively.

Determination Of The True Coincidence Spectrum

The definition of the Trues, T is given as $T = C - A$

Notations:

T: Trues

A: Accidental Counts

S: Singles CountsC : Coincidence Counts

Here, we replace A with K.S where $K = \sum A / \sum S$. This helps in improving the statistics.

Error Bar (T) = Error Bar (C) + Error Bar (A)

Error Bar (A) being negligible, Error Bar (T) = Error Bar (C)

Calculation Of Chi-Squared

The chi-squared difference between A and K.S. is

$$\chi^2 = \frac{\sum_{i=1}^{N} \frac{(K.S_i - A_i)^2}{K.S_i}}{N-1}$$

Here, i is the number of points of the N-point spectrum. χ^2 is normalized to unity., with a 1-σ error bar of $2/\sqrt{N}$. If χ^2 deviates from 1 by significantly more than $2/\sqrt{N}$, it indicates something non-statistically wrong with the measurement apparatus which needs to be corrected before proceeding.

APPENDIX D

EXTRAPOLATION OF RAMAKER FUNCTION CONSTANTS

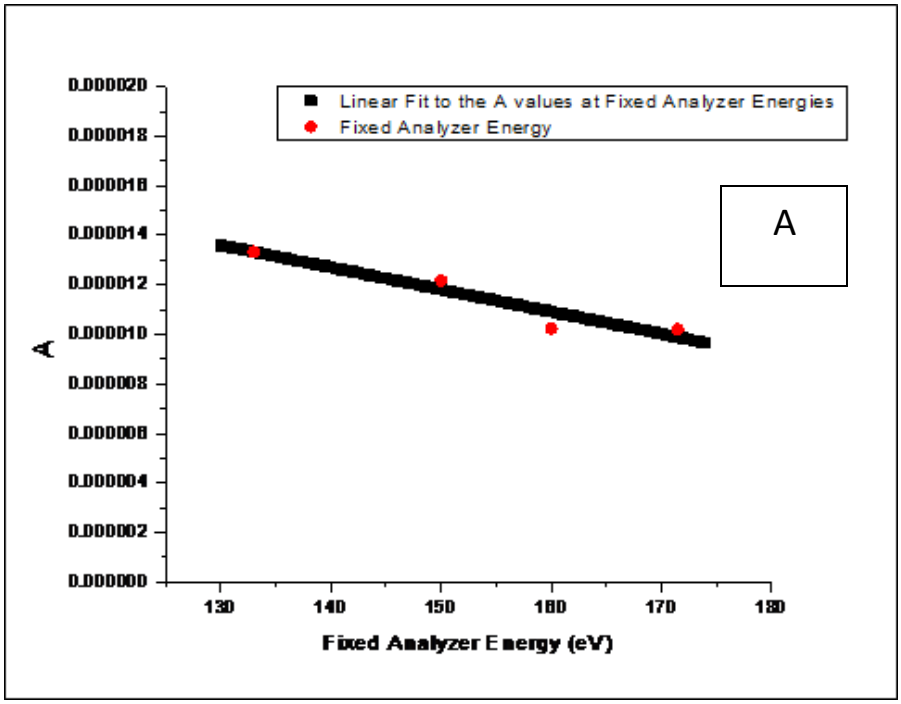

Figure D1 Extrapolation of Ramaker Constant 'A' to 133 eV

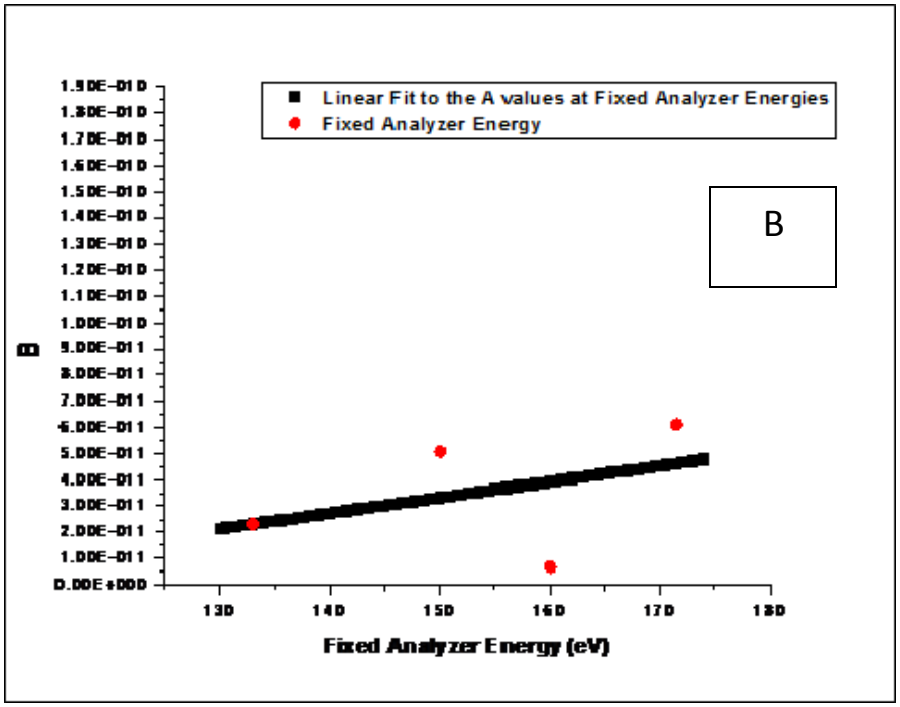

Figure D2 Extrapolation of Ramaker Constant 'B' to 133 eV

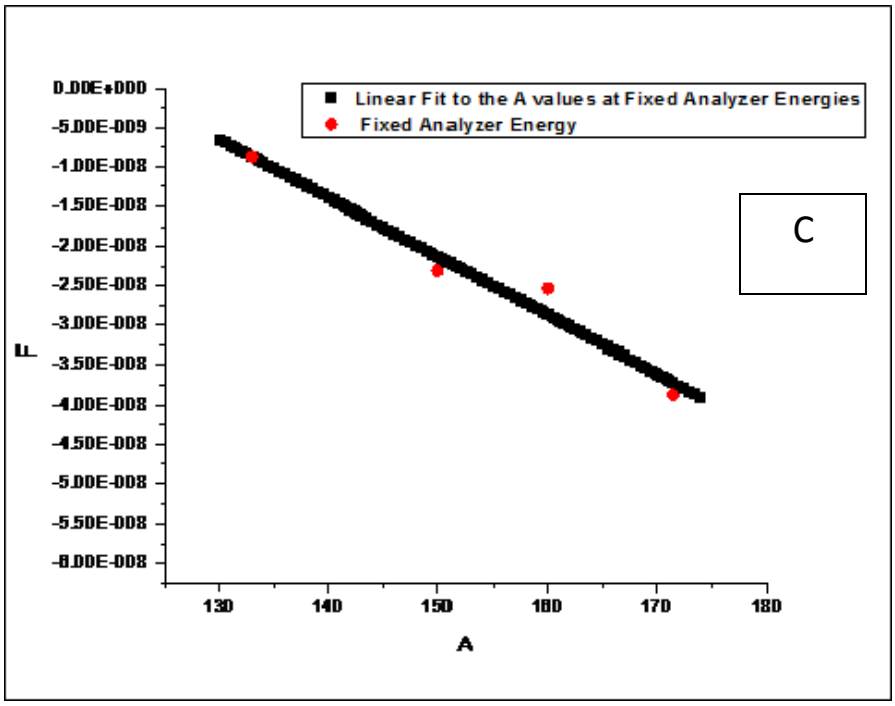

Figure D3 Extrapolation of Ramaker Constant 'C' to 133 eV

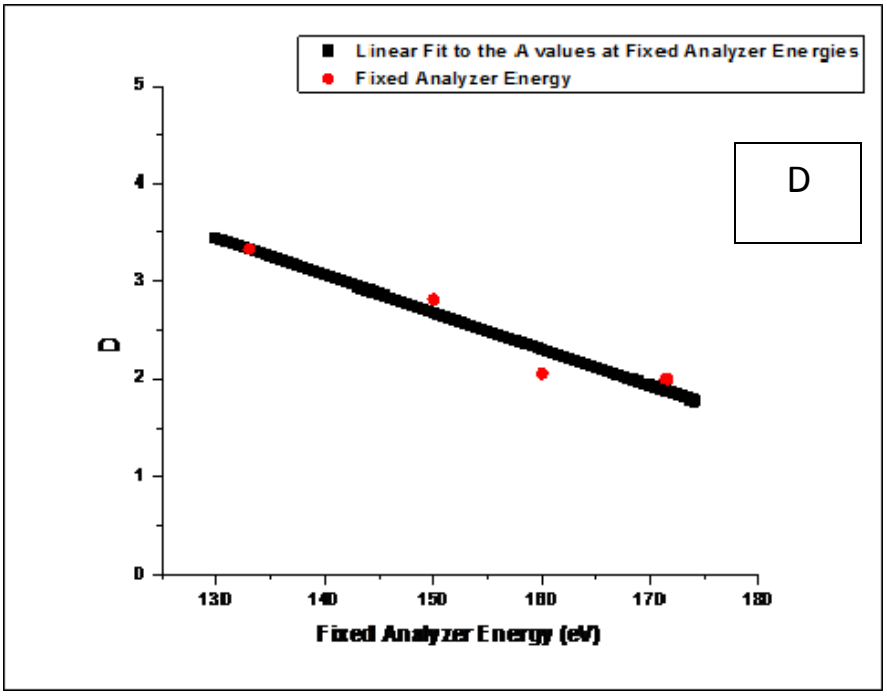

Figure D4 Extrapolation of Ramaker Constant 'D' to 133 eV

REFERENCES

1 E.H.S. Burhop, The Auger Effect and other Radiationless Transitions, (Cambridge Univ. Press, (1952)

2 W.Mehlhorn, “The Auger Effect” Report from the Behlen lab of Phys., Univ. of Nebraska (1970).

3 X-Ray Data Booklet. Lawrence Berkeley National Laboratory

4 Giorgio Margaritondo, Introduction to Synchrotron Radiation, (Oxford University Press, 1988).

5 C. J. Powell, Phys. Rev. Lett. **38**, 1429 (1977)

6 C.O.Almbladh, A.L.Morales, and G.Grossmann. Phys. Rev. B, **39**,3489 (1989)

7 E.Jensen, R.A.Bartynski, S.L.Hulbert and E.D.Johnson, Review of Scientific Instruments, **63**, (1992) 3013-26

8 R.A.Bartynski, E. Jensen, S.L. Hulbert, and C.C.Kao, Progress in Surface Science, **53**, 155-162, (1996)

9 J. A. R. Samson, Techniques of Vacuum Ultraviolet Spectroscopy (John Wiley and Sons, New York, 1967).

10 H. W. Haak, G. A. Sawatzky, and T. D. Thomas, Physics Review Letters, **41**, (1978), 1825-7.

11 Physical electronics Corporation model 255-G

12 Giorgio Margaritondo, Introduction to Synchrotron Radiation (Oxfort University Press 1988).

13 D. E. Ramaker, J. S. Turner and N. H. Turner, J. Elect. Spec., **17**, 45-65, (1979)

14 M. P. Seah, Surface Sci., **17**, 132, (1969)

15 M. Inokuti, Rev. Mod. Phys., **43**, 297, (1971)

16 R. Sundaramoorthy, First Direct Measurement of the Energy Spectra of Individual Auger Cascade Steps in Solids, Univ. of Texas Arlington.

17 Practical Surface Analysis, M. P Seah and D. Briggs, 1, (John Wiley & Sons, New York 1990)

BIOGRAPHICAL INFORMATION

Sushant Kalaskar did his undergraduate studies majoring in Polymer Engineering from the University of Pune, India during the years 2003 – 2007 and graduated with a First class. Completing his senior year project at National Chemical Laboratory of India, Pune, he worked as Project Engineer at TATA Autocomp Systems Ltd., India in the year 2008. In the Fall of 2008, he gained admission to the University of Texas at Arlington (UTA) for his Master of Science degree in Materials Science and Engineering. He joined the Department of Physics as a Graduate Research Assistant in January 2009, a step towards completion of his Masters level Thesis. He performed his MS research at the National Synchrotron Light Source (NSLS), Brookhaven National Laboratory (BNL), New York on “Auger Photoelectron Coincidence Spectroscopy” under the guidance of Dr. Alex Weiss of UTA and Dr. Steven Hulbert of NSLS, BNL. He graduated in December 2010 from UTA. He has diverse academic interests including Solar cell catalyst research, Surface studies, Semiconductor fabrication, Polymer processing and characterization.